Quantum dynamics, isotope effects, and power spectra of H_2^+ and HD^+ excited to the continuum by strong one-cycle laser pulses: Three-dimensional non-Born-Oppenheimer simulations

Guennaddi K. Paramonov,[1] Tillmann Klamroth,[1] H. Z. Lu,[2] and André D. Bandrauk[2]
[1]*Institut für Chemie, Universität Potsdam, Karl-Liebknecht-Strasse 24-25, 14476 Potsdam-Golm, Germany*
[2]*Université de Sherbrooke, Laboratoire de Chimie Théorique, Faculté des Sciences, Université de Sherbrooke, Sherbrooke, Québec, Canada J1K 2R1*

(Received 8 November 2018; published 27 December 2018)

Non-Born-Oppenheimer quantum dynamics of H_2^+ and HD^+ excited by single one-cycle laser pulses linearly polarized along the molecular (z) axis have been studied within a three-dimensional model, including the internuclear distance R and electron coordinates z and ρ, by means of the numerical solution of the time-dependent Schrödinger equation on the timescale of about 200 fs. Laser carrier frequencies corresponding to the wavelengths of $\lambda_l = 400$ and 50 nm have been used and the amplitudes of the pulses have been chosen such that the energies of H_2^+ and HD^+ are above the dissociation threshold after the ends of the laser pulses. It is shown that excitation of H_2^+ and HD^+ above the dissociation threshold is accompanied by formation of vibrationally "hot" and "cold" ensembles of molecules. Dissociation of vibrationally "hot" molecules does not prevent the appearance of post-laser-pulse electronic oscillations, parallel z oscillations, and transversal ρ oscillations. Moreover, dissociation of "hot" molecules does not influence characteristic frequencies of electronic z and ρ oscillations. The main difference between the laser-induced quantum dynamics of homonuclear H_2^+ and its heteronuclear isotope HD^+ is that fast post-laser-pulse electronic z oscillations in H_2^+ are regularly shaped with the period of $\tau_{shp} \approx 30$ fs corresponding to nuclear oscillations in H_2^+, while electronic z oscillations in HD^+ arise as "echo pulses" of its initial excitation and appear with the period of $\tau_{echo} \approx 80$ fs corresponding to nuclear motion in HD^+. Accordingly, corresponding power spectra of nuclear motion contain strong low-frequency harmonics at $\omega_{shp} = 2\pi/\tau_{shp}$ in H_2^+ and $\omega_{echo} = 2\pi/\tau_{echo}$ in HD^+. Power spectra related to both electronic and nuclear motion have been calculated in the acceleration form. Both higher- and lower-order harmonics are generated at the laser wavelength $\lambda_l = 400$ nm, while only lower-order harmonics are well pronounced at $\lambda_l = 50$ nm. It is also shown that a rationalized harmonic order, defined in terms of the frequency of the laser-induced electronic z oscillations, agrees with the concept of inversion symmetry for electronic motion in diatomic molecules.

DOI: 10.1103/PhysRevA.98.063431

I. INTRODUCTION

According to the well-known, electron–parent ion, recollision model of Corkum [1], initially related to strong-field ionization of atoms, an ionized atom does not become free from the laser-driven electron immediately. Instead, there is a significant probability for the electron to return back to the parent ion during several optical cycles of the laser field due to the electron-field following, i.e., multiple recollisions of the laser-driven electron and the parent ion occur. This model was able to predict a cutoff in high-order harmonic generation, double ionization, and high-energy above-threshold ionization [1]. A fully quantum theory of high-order harmonic generation by atoms excited with low-frequency laser fields was reported one year later [2]. Subsequently, a perfect electron-field following was predicted to occur during many optical cycles in molecular ions H_2^+ and HD^+ excited by the infrared laser field [3,4]. Excitation of molecules with lasers induces both electronic and nuclear motion, which influence each other as well [3,4]. Accordingly, recollisions of laser-driven electrons with the rest of a molecule are much more complicated as compared to atoms, resulting in a more complicated process of high-order harmonic generation [5,6]. In its turn, high-order harmonic generation in molecules [7] can be used to reveal electronic, nuclear, vibrational, and rotational dynamics of molecules and their orientation. In fact, the Corkum recollision model [1] has finally led to a new field of recollision physics [8] that unites laser and collision physics.

An interesting question of free evolution of laser-excited molecules after the driving laser pulse is over was addressed in our previous works [9–12], where non-Born-Oppenheimer time-dependent quantum numerical simulations predicted the existence of post-laser-pulse oscillations of binding particles, both electrons [9,11,12] and muons [10]. It was also shown that post-laser-pulse electronic oscillations in H_2^+ are well correlated with periodic elongations and contractions of the internuclear distance [11,12]. The possibility of higher-order harmonic generation was shown for both electronic (T_2^+, H_2^+) and muonic ($dd\mu$, $dt\mu$) molecular ions (see Refs. [9,11,12] and Ref. [10], respectively). Moreover, in the case of H_2^+ excited close to the dissociation threshold by one-cycle laser pulse, both higher- and lower-order harmonics were generated [12].

In this work, we extend our previous investigations [12] from the homonuclear H_2^+ ion to its inhomonuclear isotope HD^+ and consider the case of higher excitation energy. Since

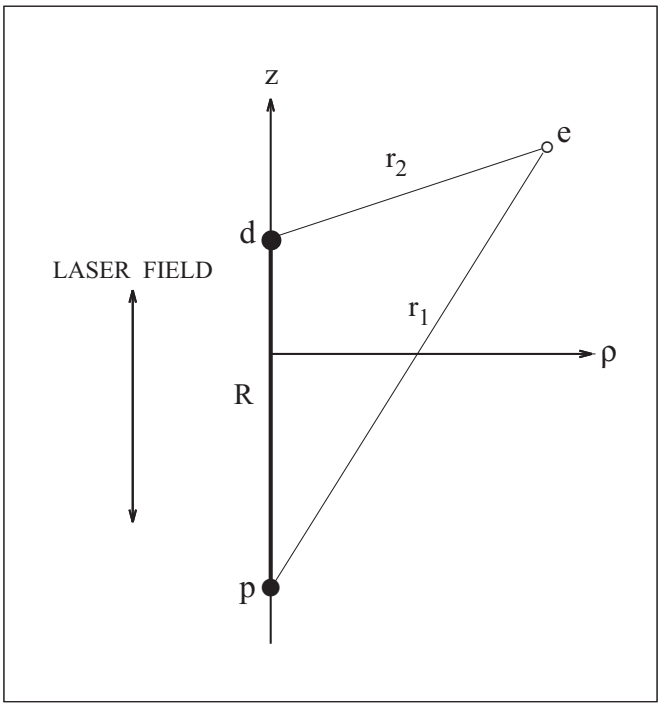

FIG. 1. The three-body 3D model of HD^+ excited by a laser field linearly polarized along the z axis. The internuclear separation is R, the distances between the electron (e) and each of the two nuclei, p and d, are r_1 and r_2, respectively.

the isotope substitution of one of two protons by a deuteron breaks the inversion symmetry of electron motion in simple diatomic systems [5], post-laser-pulse electronic oscillations in HD^+ may be significantly different from those occurring in $H_2{}^+$, similarly to a drastic change of the laser-driven dynamics of HD in comparison to H_2 analyzed in [5]. More specifically, we study the non-Born-Oppenheimer quantum dynamics of $H_2{}^+$ and HD^+ excited above the dissociation threshold by linearly polarized along the molecular (z) axis intense electric fields in single one-cycle laser pulses by means of the numerical solution of the time-dependent Schrödinger equation within the three-dimensional (3D) non-Born-Oppenheimer model that includes the internuclear distance R and electron coordinates z and ρ. The electron-nucleus and nucleus-nucleus Coulombic interactions are treated by making use of a nuclear drop model [13].

II. MODELS, EQUATIONS OF MOTION, AND NUMERICAL TECHNIQUES

The three-body non-Born-Oppenheimer 3D model with Coulombic interactions representing HD^+ excited by the laser field linearly polarized along the z axis is shown in Fig. 1. The nuclear motion is restricted to the polarization direction of the laser electric field, whereas the electron (e) moves in three dimensions with conservation of cylindrical symmetry. Within this model, two coordinates of the electron, z and ρ, measured with respect to the center of mass of proton (p) and deuteron (d), are treated explicitly together with the internuclear separation R.

The heteronuclear HD^+ system has a permanent dipole moment. The component of the dipole moment along the z axis is defined [14] by

$$d_z(R,z) = -e\{R(M_\mathrm{d} - M_\mathrm{p})/(M_\mathrm{d} + M_\mathrm{p}) + z[1 + M_\mathrm{e}/(M_\mathrm{d} + M_\mathrm{p} + M_\mathrm{e})]\}, \quad (1)$$

where e is the electron charge, M_d, M_p, and M_e are the deuteron, proton, and electron masses, respectively. Since HD^+ possesses a permanent dipole moment, its vibrational motion is excited both directly, by the laser field, and nonadiabatically, due to the electron motion [3,4]. At the same time, the laser-driven electronic motion along the optically active z degree of freedom induces electronic motion along the optically passive transversal ρ degree of freedom due to the 3D wave properties of the electron [3,4].

In contrast, the homonuclear $H_2{}^+$ system does not have a permanent dipole moment. The component of the dipole moment of $H_2{}^+$ along the z axis is simply

$$d_z(z) = -ez[1 + M_\mathrm{e}/(2M_\mathrm{p} + M_\mathrm{e})]. \quad (2)$$

Therefore, vibrational motion in $H_2{}^+$ is excited only indirectly, due to the electronic motion induced by the laser field along the z axis [3,4]. Electronic motion along the optically passive transversal ρ degree of freedom is induced only due to the 3D wave properties of an electron and its laser-driven motion along the optically active z axis.

The time-dependent Schrödinger equation (TDSE) governing the quantum dynamics of HD^+ in the classical laser field (Fig. 1) is

$$i\hbar\frac{\partial}{\partial t}\Psi = -\frac{\hbar^2}{2m_\mathrm{n}}\frac{\partial^2\Psi}{\partial R^2} - \frac{\hbar^2}{2m_\mathrm{e}}\left(\frac{\partial^2\Psi}{\partial\rho^2} + \frac{1}{\rho}\frac{\partial\Psi}{\partial\rho}\right) - \frac{\hbar^2}{2m_\mathrm{e}}\frac{\partial^2\Psi}{\partial z^2} + V(R,r_1,r_2)\Psi - d_z(R,z)\mathcal{E}(t)\Psi, \quad (3)$$

where $m_\mathrm{n} = M_\mathrm{d}M_\mathrm{p}/(M_\mathrm{d} + M_\mathrm{p})$ is the nuclear reduced mass, $m_\mathrm{e} = M_\mathrm{e}(M_\mathrm{d} + M_\mathrm{p})/(M_\mathrm{e} + M_\mathrm{d} + M_\mathrm{p})$ is the electron reduced mass, and $V(R,r_1,r_2)$ is the overall Coulomb potential

$$V(R,r_1,r_2) = V_0(R) - V_1(r_1) - V_2(r_2). \quad (4)$$

The Coulomb potentials in the right-hand side of Eq. (4) are treated within the nuclear drop model [13] as follows. For the proton-deuteron interaction, the Coulomb potential

$$V_0(R) = \frac{e^2}{r_\mathrm{p} + r_\mathrm{d}}\left[\frac{3}{2} - \frac{R^2}{2(r_\mathrm{p} + r_\mathrm{d})^2}\right] \text{ for } R \leqslant r_\mathrm{p} + r_\mathrm{d} \quad (5)$$

and $V_0(R) = 1/R$, for $R > r_\mathrm{p} + r_\mathrm{d}$, where $r_\mathrm{p} = 0.8751$ fm and $r_\mathrm{d} = 2.1413$ fm are the proton and deuteron charge radii [15], respectively.

For the electron-nucleus interactions, the electron is treated as being pointlike and two Coulomb potentials $V_k(r_k)$, $k = 1, 2$, read as

$$V_k(r_k) = \frac{e^2}{r_\mathrm{n}}\left[\frac{3}{2} - \frac{r_k^2}{2r_\mathrm{n}^2}\right] \text{ for } r_k \leqslant r_\mathrm{n} \quad (6)$$

and $V_k(r_k) = 1/r_k$, for $r_k > r_\mathrm{n}$, where the nuclear radius r_n stands for r_p or r_d, specified above, and r_k stands for

the electron-proton r_1 or electron-deuteron r_2 distances, defined by

$$r_1(R,\rho,z)=\{\rho^2+[z+RM_{\rm d}/(M_{\rm d}+M_{\rm p})]^2\}^{1/2} \quad (7)$$

and

$$r_2(R,\rho,z)=\{\rho^2+[z-RM_{\rm p}/(M_{\rm d}+M_{\rm p})]^2\}^{1/2}, \quad (8)$$

respectively (see Fig. 1).

In the case of homonuclear H_2^+, the deuteron mass $M_{\rm d}$ is replaced with the proton mass $M_{\rm p}$ with straightforward modifications of Eqs. (3)–(8). The laser field $\mathcal{E}(t)$ in Eq. (3) is chosen as a single one-cycle pulse with a smooth sine-squared shape [12]

$$\mathcal{E}(t)=\mathcal{E}_0\sin^2(\pi t/t_p)\sin(\omega_l t), \quad 0\leqslant t\leqslant t_p \quad (9)$$

where $\mathcal{E}_0$ is the amplitude, t_p is the pulse duration, and ω_l is the laser carrier frequency. Single one-cycle laser pulses are chosen here because they provide the shortest periodic excitation of a molecule and serve to test the Corkum recollision model [1] as a limiting case. Besides, strong single-cycle laser pulses proved to be a very important tool in, e.g., nonlinear optics [16]. With a symmetric shape of the laser pulse (9), its net area is zero in order to avoid static-field effects. Moreover, it is easy to show that in the current case of one-cycle pulses ($t_p=2\pi/\omega_l$), the laser field of Eq. (9) corresponds to only two carrier frequencies, ω_l and $2\omega_l$, and reads as $\mathcal{E}(t)=\mathcal{E}_0[0.5\,\sin(\omega_l t)-0.25\,\sin(2\omega_l t)]$.

Two laser carrier frequencies, ω_l, chosen for both H_2^+ and HD^+, correspond to the laser wavelengths of $\lambda_l=50$ and 400 nm. These laser frequencies have been chosen because only higher-order harmonics (measured in terms of ω_l) were generated in H_2^+ excited close from below to its dissociation threshold at $\lambda_l\geqslant 200$ nm, while both higher- and lower-order harmonics could be generated at $\lambda_l<200$ nm [12]. In particular, only lower-order harmonics were generated at $\lambda_l=50$ nm [12].

At $\lambda_l=400$ nm, corresponding to the laser carrier frequency $\omega_l=0.113\,91$ a.u. (atomic units), the laser-pulse amplitude is $\mathcal{E}_0=0.072$ a.u. (the peak intensity of the pulse is $I_0=1.82\times10^{14}$ W/cm^2) and the pulse duration is $t_p=1.33$ fs. Such laser pulses provide at the ends of the pulses the following energies: $\langle E(t_p)\rangle=-0.455\,51$ a.u. for H_2^+ and $\langle E(t_p)\rangle=-0.493\,02$ a.u. for HD^+. Hence, the final continuum energies above the dissociation energy $E_{\rm D}=-0.5$ a.u. are 0.4449×10^{-1}a.u. for H_2^+ and 0.698×10^{-2}a.u. for HD^+.

At $\lambda_l=50$ nm ($\omega_l=0.911\,27$ a.u., $t_p=0.167$ fs), the laser-pulse amplitude $\mathcal{E}_0=0.9$ a.u. ($I_0=2.84\times10^{16}$ W/cm^2) has been chosen such that the lowest final energy at the end of the pulse is close to the highest final energy at $\lambda_l=400$ nm. This choice gives the following energies at the ends of the pulses: $\langle E(t_p)\rangle=-0.455\,15$ a.u. for H_2^+ and $\langle E(t_p)\rangle=-0.427\,24$ a.u. for HD^+. Accordingly, the respective continuum energies above the dissociation energy $E_{\rm D}$ are 0.4485×10^{-1} a.u. for H_2^+ and 0.7276×10^{-1} a.u. for HD^+.

Note that the above-specified subfemtosecond at $\lambda_l=50$ nm ($\hbar\omega_l=24.8$ eV) and, especially, femtosecond at $\lambda_l=400$ nm ($\hbar\omega_l=3.1$ eV) one-cycle laser pulses are rather feasible nowadays due to recent achievements of the laser technology [17] that already led to generation of ultrashort laser pulses in the deep and vacuum ultraviolet (4-9 eV).

Numerical techniques used to solve the 3D equation of motion (3) have been described in detail in our previous works [3,4]. In particular, electronic motion along the z and ρ degrees of freedom has been treated by making use of the polynomial expansion of the wave function over the Hermite $H_n(z)$ and the Laguerre $L_m(\rho)$ polynomials, respectively, and subsequent integration on the corresponding quadrature points for calculation of the expectation values. Nuclear motion has been treated with the common split-operator method and FFT on the equidistant grid for the R degree of freedom. The dissociation probability has been calculated with the time- and space-integrated outgoing flux for the nuclear coordinate R; the ionization probabilities have been calculated with the respective fluxes separately for the positive and the negative directions of the z axis, as well as for the outer end of the ρ axis.

The size of the z grid has been chosen substantially larger than the maximum excursion of the electron along the z axis, $\alpha_z=\mathcal{E}_0/(M_{\rm e}\omega^2)$. The maximum electron excursion, that can be reached with the laser pulses used in this work, is $\alpha_z=5.55$ a.u. The choice of the z grid has been based on this value and the size of the ρ grid has been chosen accordingly. Specifically, the 3D wave packet was damped with the imaginary smooth optical potentials [18], at $z<-92$ a.u., at $z>92$ a.u., and at $\rho>98$ a.u. for the electronic motion, and at $R>25$ a.u. for the nuclear motion.

Initially, at $t=0$, both H_2^+ and HD^+ are assumed to be in their ground vibrational ($v=0$) and ground electronic ($\sigma_g 1s$) states. The wave functions of the initial states have been obtained by the numerical propagation of Eq. (3) in the imaginary time without the laser field ($\mathcal{E}_0=0$).

III. LASER-DRIVEN NON-BORN-OPPENHEIMER QUANTUM DYNAMICS AND SHORT-TERM FREE EVOLUTION OF H_2^+ AND HD^+: COMPARISON TO THE CASE OF BORN-OPPENHEIMER FIXED INTERNUCLEAR DISTANCES

In this section we present the results of the non-Born-Oppenheimer quantum dynamics of H_2^+ and HD^+ and their free evolution after the ends of laser pulses. These results are compared to those obtained at fixed internuclear distances, which is usually referred to as the Born-Oppenheimer approximation.

In Fig. 2, we present the laser-driven quantum dynamics of H_2^+ (left panel) and HD^+ (right panel) followed by their free evolution on a short timescale. The H_2^+ ion is excited at the laser wavelength of $\lambda_l=400$ nm ($\omega_l=0.113\,91$ a.u., $\mathcal{E}_0=0.072$ a.u., $t_p=1.33$ fs) and the HD^+ ion is excited at $\lambda_l=50$ nm ($\omega_l=0.911\,27$ a.u., $\mathcal{E}_0=0.9$ a.u., $t_p=0.167$ fs). The non-Born-Oppenheimer quantum dynamics of H_2^+ and HD^+ is represented by their time-dependent energies $\langle E(t)\rangle$ [Figs. 2(a) and 2(d)], expectation values $\langle z\rangle$ of the optically active electronic degree of freedom [Figs. 2(b) and 2(e)] and by the expectation values $\langle\rho\rangle$ [Figs. 2(c) and 2(f)] of the optically passive electronic degree of freedom (all plotted by curves 1

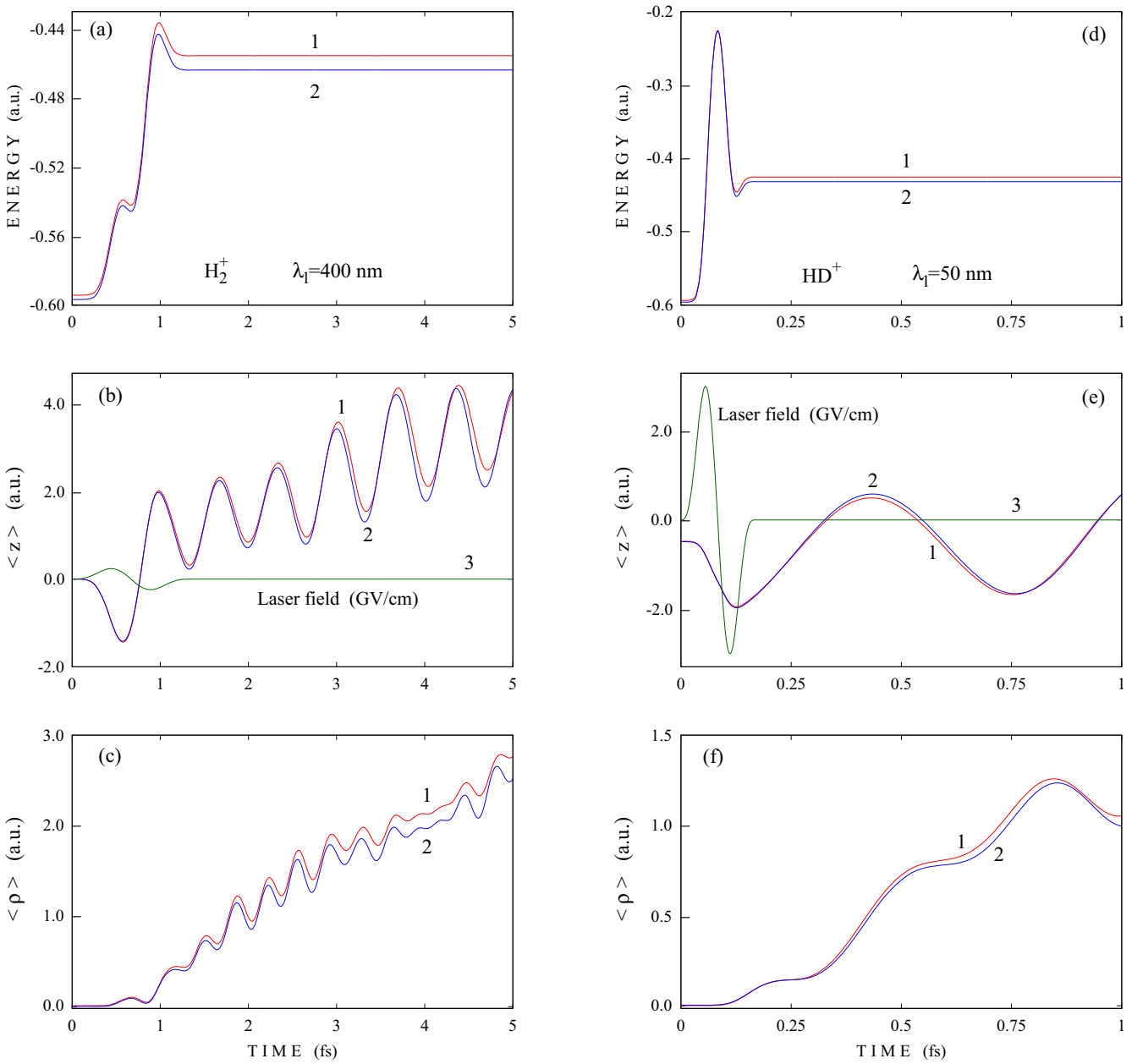

FIG. 2. Quantum dynamics of $H_2{}^+$ (left panel) and HD^+ (right panel) excited by one-cycle laser pulses followed by a short-term free evolution. (a), (d) Time-dependent energies $\langle E \rangle$; (b), (e) expectation values $\langle z \rangle$ of the laser-driven electronic degree of freedom z and applied laser fields (curves 3); (c), (f) expectation values $\langle \rho \rangle$ of the optically passive transversal electronic degree of freedom ρ.

in Fig. 2). For the sake of comparison, results obtained at a fixed internuclear distance of $R = 2$ a.u., corresponding to the classical equilibrium, are plotted in Fig. 2 by curves 2. Curves 3 in Figs. 2(b) and 2(e) represent the driving one-cycle laser pulses [the laser field presented in Fig. 2(e) is scaled down by the factor of 1.5].

The time-dependent observables presented in Fig. 2 confirm that the results obtained at a fixed internuclear distance (curves 2) are very similar to those obtained beyond the Born-Oppenheimer approximation (curves 1). An evident physical reason of such a similarity is a very short duration of the laser pulses used to excite both $H_2{}^+$ (left panel, $t_p = 1.33$ fs) and HD^+ (right panel, $t_p = 0.167$ fs). Indeed, on such short time intervals, heavy nuclei do not noticeably move and, therefore, the difference between the results obtained in both cases is very small.

Other important features of the results shown in Fig. 2 are as follows. The energies gained by $H_2{}^+$ and HD^+ [Figs. 2(a) and 2(d)] are very high in the second halves of one-cycle laser pulses (e.g., up to -0.23 a.u. in the case of HD^+) and remain above their dissociation threshold, $E_D = -0.5$ a.u., after the ends of the pulses. Such high excitation was one of the focuses of this work.

Expectation values $\langle z \rangle$ of the laser-driven electron degree of freedom z follow the applied laser field out of phase ($\langle z \rangle$ decreases when the field strength increases) only approximately

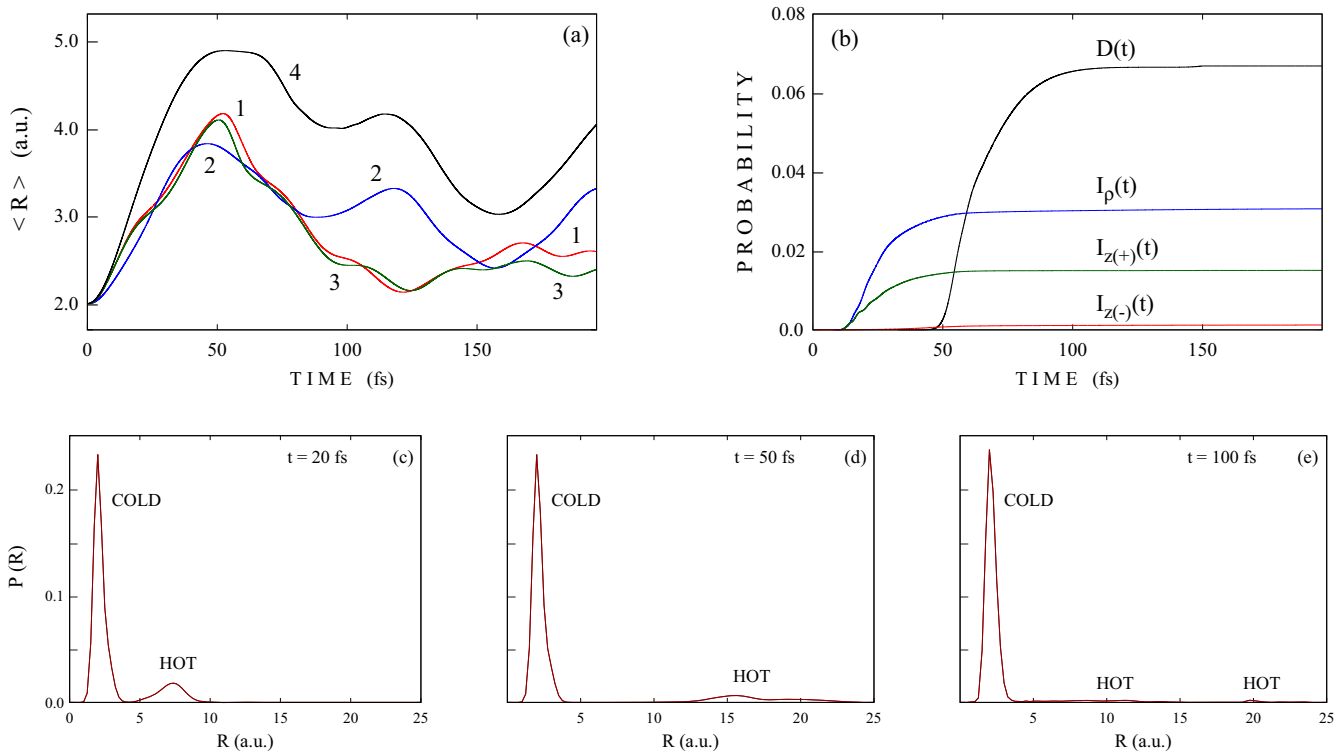

FIG. 3. (a) Time-dependent internuclear distances in H_2^+ and HD^+ excited at the laser wavelength of 400 and 50 nm: curves 1 and 2 represent H_2^+ and HD^+ at $\lambda_l = 400$ nm, curves 3 and 4 represent H_2^+ and HD^+ at $\lambda_l = 50$ nm. (b) Ionization and dissociation probabilities of H_2^+ at $\lambda_l = 400$ nm: curve D(t), dissociation; $I_\rho(t)$, ionization from the outer end of the ρ axis; $I_{z(\pm)}(t)$, ionization in the positive and negative directions of the z axis. (c), (d), (e) Formation of vibrationally cold and hot ensembles of H_2^+ excited at $\lambda_l = 400$ nm: probability density $P(R)$ of Eq. (10) well before dissociation (c), at the beginning (d) and close to the end of dissociation (e).

in H_2^+ [Fig. 2(b)] and only rather roughly in HD^+ Fig. 2(e)]. As a result, electronic motion along the z coordinate remains excited at the end of the pulse and post-laser-pulse electronic z oscillations with characteristic frequencies $\omega_z^{\rm osc}$ occur in both H_2^+ and HD^+.

The optically passive transversal electronic degree of freedom ρ is excited only due to the wave properties of the electron which is driven along the z axis by the applied laser field. In homonuclear H_2^+ [Fig. 2(c)], expectation values $\langle\rho\rangle$ of the electron approximately follow the laser field of Fig. 2(b) in phase during the laser pulse and, therefore, oscillate with the frequency of $\omega_\rho^1 \approx \omega_z^{\rm osc}$ at $0 \leqslant t \leqslant t_p = 1.33$ fs, while after the end of the pulse, they demonstrate post-laser-pulse ρ oscillations which are approximately twice as fast as electronic z oscillations, i.e., the respective frequency of ρ oscillations is $\omega_\rho^{(2)} \approx 2\omega_z^{\rm osc}$. This effect was explained in Refs. [3,4] by the fact that excitation of the ρ degree of freedom takes place at every half-cycle of the laser field, i.e., at every turning point of the laser-driven electronic oscillations along the z axis. The effect also occurs during electronic post-laser-pulse free oscillations [11,12] and has been referred to as the "frequency doubling" of electronic ρ oscillations. In heteronuclear HD^+ [Fig. 2(f)], only ρ oscillations with the frequency $\omega_\rho^{(2)} \approx 2\omega_z^{\rm osc}$ are well pronounced after the end of the pulse [Fig. 2(e)], while the ρ oscillations with the frequency $\omega_\rho^{(1)} \approx \omega_z^{\rm osc}$ appear at a later time, as it will be clearly seen, e.g., from Fig. 6(f) presented later.

IV. DISSOCIATION AND INTERNUCLEAR DISTANCE: FORMATION OF VIBRATIONALLY COLD AND HOT ENSEMBLES OF MOLECULES. ELECTRONIC z OSCILLATIONS AND NUCLEAR MOTION

Since the laser pulses have been chosen such as to excite H_2^+ and HD^+ above the dissociation threshold, the time-dependent internuclear distance R and the role of dissociation may be very important and should, therefore, be analyzed in detail. In Fig. 3(a), time-dependent expectation values $\langle R\rangle$ of the internuclear distance in H_2^+ and HD^+ excited at the laser wavelength $\lambda_l = 400$ nm are presented by curves 1 and 2, respectively. Curve 3 (representing H_2^+) and curve 4 (representing HD^+) correspond to the case of the laser wavelength $\lambda_l = 50$ nm. It is clearly seen that in all four cases, the internuclear distance reaches its maximum at about $t \approx 50$ fs and decreases later on, demonstrating several oscillations.

In Fig. 3(b), time-dependent ionization and dissociation probabilities are plotted for the case when H_2^+ is excited at the laser wavelength of $\lambda_l = 400$ nm. Curves $I_\rho(t)$, $I_{z(+)}(t)$, and $I_{z(-)}(t)$ correspond to ionization from the outer end of the ρ axis and from the positive and the negative directions of the z axis, respectively. Curve D(t) represents the time-dependent dissociation of H_2^+. It is seen that ionization starts prior to dissociation and the ionization probability from the outer end of the ρ axis is larger than those from both the positive and the negative directions of the z axis. It can be explained by

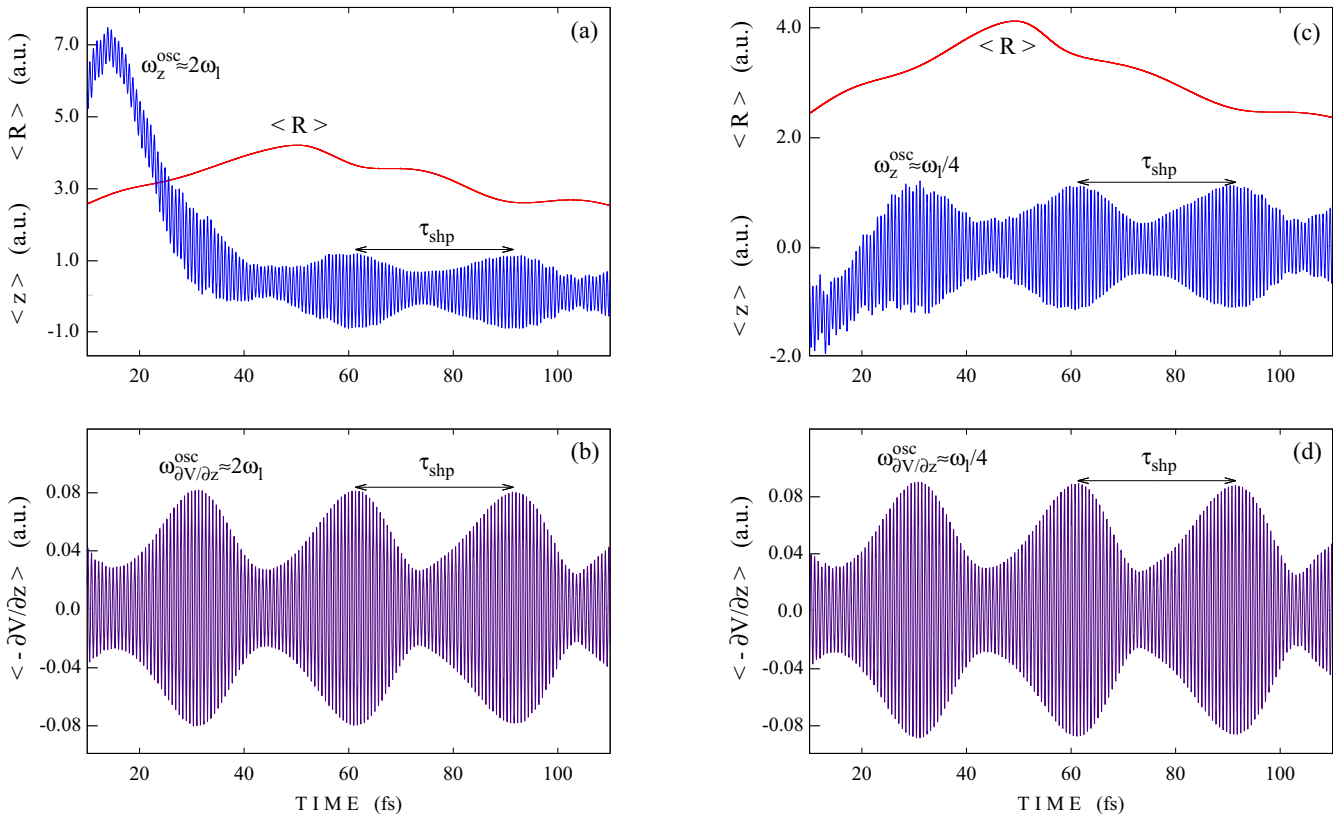

FIG. 4. Post-laser-pulse electronic z oscillations in H_2^+ excited at the laser wavelength $\lambda_l = 400$ nm (left panel) and at $\lambda_l = 50$ nm (right panel): (a), (c) time-dependent expectation values $\langle R \rangle$ and $\langle z \rangle$; (b), (d) time-dependent expectation values $\langle -\partial V/\partial z \rangle$. Parameters of the one-cycle laser pulses are: $\mathcal{E}_0 = 0.072$ a.u. ($I_0 = 1.82 \times 10^{14}$ W/cm^2), $\omega_l = 0.11391$ a.u. and $t_p = 1.33$ fs at $\lambda_l = 400$ nm; $\mathcal{E}_0 = 0.9$ a.u. ($I_0 = 2.84 \times 10^{16}$ W/cm^2), $\omega_l = 0.91127$ a.u. and $t_p = 0.167$ fs at $\lambda_l = 50$ nm.

the aforementioned effect of frequency doubling of electronic ρ oscillations [12], i.e., by the fact that electronic density is delocalized in the ρ direction at every turning point of electronic z oscillations when the electron changes the direction of its motion along the z axis, i.e., twice per every cycle of electronic z oscillations [3,4]. Thus, the rate of ionization from the outer end of the ρ axis is increased as compared to those from the positive and the negative directions of the z axis. In three other cases studied in this work (HD^+ excited at $\lambda_l = 400$ nm, and H_2^+ and HD^+ excited at $\lambda_l = 50$ nm) the time-dependent dissociation and ionization probabilities are similar to those presented in Fig. 3(b), with the only difference that at $\lambda_l = 50$ nm ionization probabilities in the positive and negative directions of the z axis are rather close to each other.

The time-dependent dissociation probability, presented in Fig. 3(b) by curve D(t), shows that significant dissociation starts at $t \approx 50$ fs and it is for the most part completed at $t > 100$ fs. A more detailed description of vibrational excitation and dissociation can be provided by the probability density $P(R, t)$:

$$P(R,t) = \int_0^\infty \rho \, d\rho \int_{-\infty}^{\infty} dz |\Psi(R, \rho, z, t)|^2, \qquad (10)$$

which can be calculated at any time t and gives the probability to find a system at a specified internuclear distance R at any values of other two coordinates ρ and z.

In Figs. 3(c)–3(e), probability densities $P(R, t)$ of Eq. (10) calculated well before dissociation ($t = 20$ fs), at the beginning of dissociation ($t = 50$ fs), and at the end of dissociation ($t = 100$ fs) are plotted for the case when H_2^+ is excited at $\lambda_l = 400$ nm. It is clearly seen that excitation of H_2^+ is accompanied by the formation of vibrationally cold and hot ensembles. Similar behavior occurs in H_2^+ at $\lambda_l = 50$ nm and during the excitation of HD^+ at both $\lambda_l = 50$ and 400 nm as well. It is seen from Figs. 3(c)–3(e) that the cold ensemble does not substantially change its position and shape, while the hot ensemble moves towards large R, where a part of it is damped by the imaginary absorbing potential at $R > 25$ a.u. Formation of vibrationally cold and hot ensembles of molecules was first experimentally observed for SF_6 and CF_3I [19]. It was shown recently [11] that formation of vibrationally cold and hot ensembles can also take place in H_2^+ excited slightly below the dissociation threshold by two-cycle laser pulses at $\lambda_l = 200$ and 800 nm.

In order to estimate the influence of a remarkable increase of the internuclear distance at $t \approx 50$ fs [Fig. 3(a)] and dissociation on the time interval 50 fs $\leqslant t \leqslant$ 100 fs [Fig. 3(b)] on the laser-induced electronic z oscillations, we plot in Fig. 4 time-dependent expectation values $\langle z \rangle$ and $\langle R \rangle$ together with the so-called "field-free" accelerations $d^2\langle z \rangle/dt^2 = m_e^{-1}\langle -\partial V/\partial z \rangle$ of H_2^+, wherein the laser field is not taken into account, the electron mass $m_e = 1$ a.u., and the overall Coulomb potential $V(R, r_1, r_2)$ is defined by Eq. (4). It is seen from Fig. 4(a),

where expectation values $\langle z\rangle$ and $\langle R\rangle$ are presented, that the electron first makes quite a considerable excursion of more than 7 a.u. in the positive direction of the z axis and approaches $\langle z\rangle = 0$ at about $t \approx 50$ fs. It is also seen that at the maximum of the aforementioned excursion, a slowly varying expectation value $\langle z\rangle$ is modulated with very fast small-amplitude z oscillations that occur at a certain characteristic frequency $\omega_z^{\rm osc}$. At the end of the excursion, the amplitude of the fast oscillations increases and $\omega_z^{\rm osc}$ starts to play the role of a "carrier" frequency of temporally shaped electronic z oscillations proceeding around $\langle z\rangle = 0$. In contrast, the time-dependent acceleration $\langle -\partial V/\partial z\rangle$, shown in Fig. 4(b), from the very beginning appears as temporally shaped oscillations around $\langle \partial V/\partial z\rangle = 0$ occurring with the carrier frequency equal to the frequency of electronic z oscillations $\omega_z^{\rm osc}$. Moreover, the value of the characteristic frequency $\omega_z^{\rm osc}$ does not change on the time interval of Figs. 4(a) and 4(b) that includes the domain of significant dissociation of H_2^+, i.e., 50 fs $\leqslant t \leqslant$ 100 fs [Fig. 3(b)]. We can conclude, therefore, that the elongation of the internuclear distance in H_2^+ and its dissociation do not influence the characteristic frequency $\omega_z^{\rm osc}$ of electronic z oscillations, i.e., the frequency of electron recollisions with the parent ion.

Very similar electronic z oscillations, occurring with the same characteristic frequency $\omega_z^{\rm osc}$, take place if H_2^+ is excited by much stronger one-cycle laser pulse at $\lambda_l = 50$ nm, as shown in Figs. 4(c) and 4(d). The only difference is that the initial excursion of the electron is shorter and proceeds in the negative direction of the z axis. A closer look at the results presented in Fig. 4 shows that the period of characteristic z oscillations of an electron is $\tau_z^{\rm osc} = 0.689\,65$ fs, which corresponds to the frequency of $\omega_z^{\rm osc} = 0.220\,37$ a.u.

In the case of $\lambda_l = 400$ nm [Figs. 4(a) and 4(b)], the characteristic frequency of electronic z oscillations is approximately twice as large as the laser carrier frequency: $\omega_z^{\rm osc}/\omega_l = 1.935$, which corresponds to the second *higher-order* harmonic of ω_l, as explicitly indicated in Figs. 4(a) and 4(b). In contrast, in the case of $\lambda_l = 50$ nm, the relation is opposite: $\omega_z^{\rm osc}/\omega_l = 0.242$, which corresponds to the fourth *lower-order* harmonic of ω_l, as explicitly indicated in Figs. 4(c) and 4(d). The fact that single atoms or molecules may emit harmonics that are not pure integer multiples of the laser carrier frequency due to resonance effects was already discussed in Refs. [5,20] for the generation of higher-order harmonics. We can conclude from the example given above that the same holds true for the generation of lower-order harmonics. Power spectra generated by H_2^+ and HD^+ will be discussed in more detail in separate sections below. Here, we just admit that despite the fact that only one recollision is induced by one-cycle laser pulses, both higher- and lower-order harmonics may be generated.

It is also seen from Fig. 4 that post-laser-pulse fast oscillations of $\langle -\partial V/\partial z\rangle$ [Figs. 4(b) and 4(d)] and $\langle z\rangle$ at $t > 50$ fs [Figs. 4(a) and 4(c)] are temporally shaped with the period of $\tau_{\rm shp} \approx 30$ fs. Moreover, shaped electronic z oscillations are well correlated with periodic contraction and elongation of the bond length $\langle R\rangle$: local minima of $\langle R\rangle$ at around of $t \approx 60$ fs and $t \approx 90$ fs correspond to the domains of large-amplitude oscillations of $\langle z\rangle$ and $\langle -\partial V/\partial z\rangle$, while local maxima of $\langle R\rangle$ at around of $t \approx 75$ and 105 fs correspond to small-amplitude oscillations of $\langle z\rangle$ and $\langle -\partial V/\partial z\rangle$. In fact, this shaping of electronic motion is caused by nuclear motion and electron-nuclei Coulombic interactions. This was analyzed for H_2^+ excited below its dissociation threshold in our previous works [11,12] and will be discussed in detail in terms of nuclear acceleration $d^2\langle R\rangle/dt^2$ in the next section.

Note that nuclear vibrations in H_2^+ occurred with similar, yet shorter, as compared to $\tau_{\rm shp} \approx 30$ fs of Fig. 4, periods have also been calculated in previous works [21–23] devoted to vibrationally mediated dissociation, ionization, and high-order harmonic generation triggered with time-delayed laser pulses. For example, when a superposition of the two lowest vibrational states, $v = 0$ and 1, prepared with equal probabilities was chosen as the initial state of H_2^+, calculated time-dependent internuclear distance and intensity of high harmonics changed with the period of 18–19 fs [23]. At a higher initial vibrational excitation of H_2^+ achieved by pumping vibrational state $|v = 9\rangle$ with a rather weak 2400-nm laser pulse that was followed by a stronger time-delayed 1600-nm pulse, calculated dissociation and ionization probabilities changed with the period of 23–27 fs [23]. Since the period of nuclear oscillations definitely increases with the level of vibrational excitation of H_2^+, we can conclude that in our case (Fig. 4) rather high vibrational states can be involved yielding $\tau_{\rm shp} \approx 30$ fs for the period of nuclear vibrations in H_2^+.

Since inversion symmetry in HD^+ is broken, we can expect that both electronic and nuclear motion in HD^+ can be very different from those occurred in H_2^+. Nuclear motion in HD^+ is illustrated in Fig. 5, where time-dependent expectation values $\langle z\rangle$ and $\langle -\partial V/\partial z\rangle$ of HD^+ are presented together with the internuclear distance $\langle R\rangle$. Left panel corresponds to the case of $\lambda_l = 400$ nm, right panel to the case of $\lambda_l = 50$ nm. Indeed, it is seen from Fig. 5 that two local minima of $\langle R\rangle$ at around $t \approx 80$ and 160 fs well correspond to the respective domains of large-amplitude oscillations of both $\langle z\rangle$ and $\langle -\partial V/\partial z\rangle$ at both laser wavelengths used in our simulations. In contrast, the local maximum of the bond length $\langle R\rangle$ at $t \approx 120$ fs corresponds to rather small amplitudes of oscillations of both $\langle z\rangle$ and $\langle -\partial V/\partial z\rangle$.

The aforementioned correlation between the bond length $\langle R\rangle$ and expectation values $\langle z\rangle$ and $\langle -\partial V/\partial z\rangle$ of the electron can be explained by the electron-nuclei Coulombic interactions as follows. At the contraction of the bond length $\langle R\rangle$ [Figs. 5(a) and 5(c)], nuclei come close to each other and the Coulomb force $\langle -\partial V/\partial z\rangle$ acting on the electron increases [Figs. 5(b) and 5(d)], giving rise to the increase of the amplitudes of electronic z oscillations [Figs. 5(a) and 5(c)]. On the other hand, at the increasing amplitude of electronic z oscillations, the electron becomes more and more delocalized, electron density between two nuclei is thus decreased, enabling the Coulombic repulsion of nuclei to act more and more efficiently, such as to change finally from the bond contraction to bond elongation, etc. It is also clear that heavy nuclei do not respond to every fast oscillation of the light electron, and the bond length $\langle R\rangle$ approximately follows only the envelope of electronic fast oscillations. Therefore, nuclear motion and electronic z oscillations influence each other, and the overall non-Born-Oppenheimer quantum

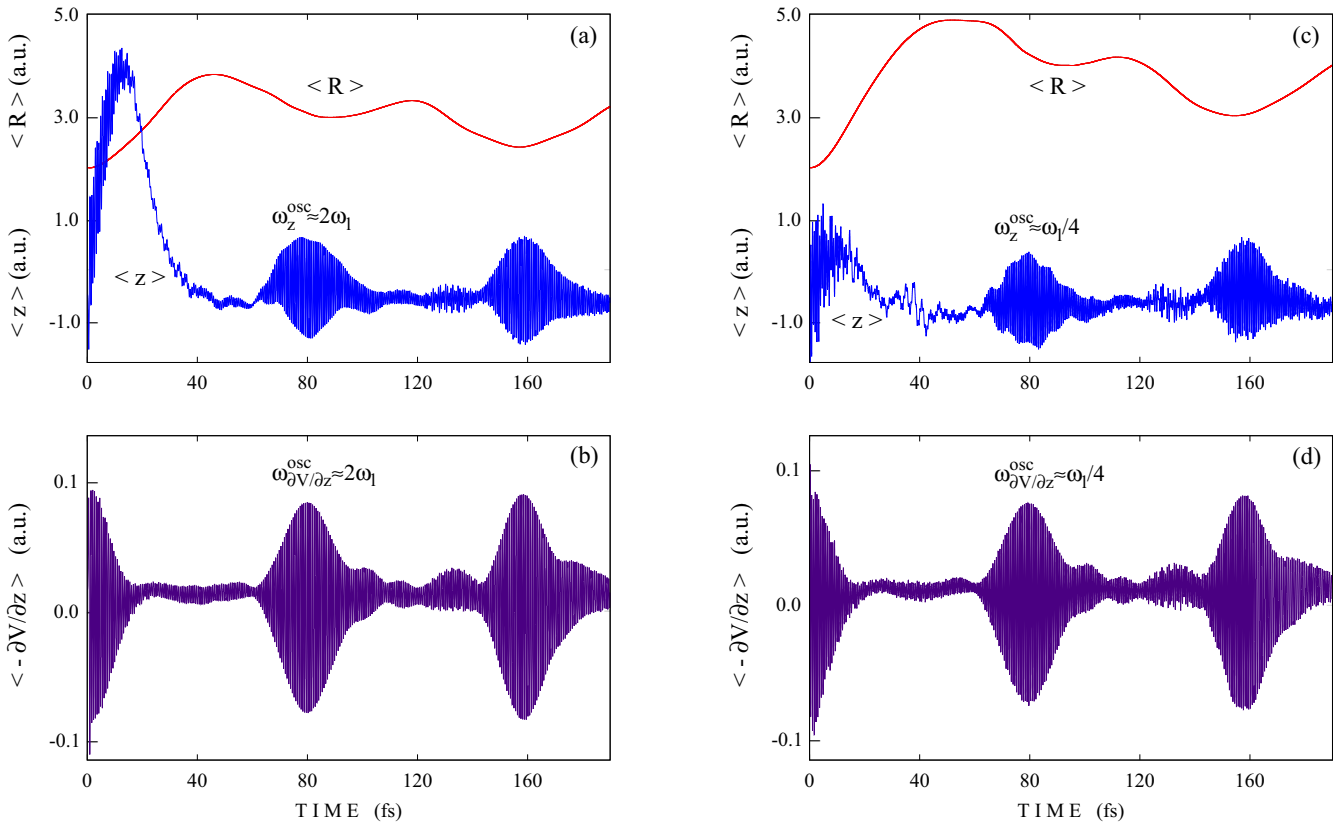

FIG. 5. Electronic z oscillations in HD^+ excited at the laser wavelength $\lambda_l = 400$ nm (left panel) and at $\lambda_l = 50$ nm (right panel): (a), (c) time-dependent expectation values $\langle R\rangle$ and $\langle z\rangle$; (b), (d) time-dependent expectation values $\langle -\partial V/\partial z\rangle$. Parameters of the one-cycle laser pulses are as in Fig. 4.

dynamics represents a combined effect of all degrees of freedom.

It is seen from the comparison of Figs. 4 and 5 that post-laser-pulse electronic z oscillations in heteronuclear HD^+ are different from those occurring in homonuclear $H_2{}^+$. Indeed, time-dependent expectation values $\langle z\rangle$ [Figs. 5(a) and 5(c)] and $\langle -\partial V/\partial z\rangle$ [Figs. 5(b) and 5(d)] appear in HD^+ as "echo pulses" of initial excitation, being separated from each other by the time interval of about 80 fs, where the amplitude of electronic z oscillations is rather small. It is easy to find that in the time domains of "echo pulses" the period of electronic z oscillations [Figs. 5(a) and 5(c)] is $\tau_z^{\rm osc} = 0.645\,16$ fs, which corresponds to the characteristic frequency $\omega_z^{\rm osc} = 0.235\,57$ a.u. Moreover the oscillations of electron acceleration $\langle -\partial V/\partial z\rangle$ occur at the same characteristic frequency of $\omega_z^{\rm osc} = 0.235\,57$ a.u. in the time domains of the corresponding "echo pulses" [Figs. 5(b) and 5(d)]. Although the characteristic frequency of z oscillations in HD^+ is higher than that in $H_2{}^+$ ($\omega_z^{\rm osc} = 0.220\,37$ a.u.), it also approximately corresponds to the second *higher-order* harmonic of ω_l at the laser wavelength of $\lambda_l = 400$ nm ($\omega_z^{\rm osc}/\omega_l = 2.068$), and to the fourth *lower-order* harmonic at $\lambda_l = 50$ nm ($\omega_z^{\rm osc}/\omega_l = 0.2585$), as indicated in Fig. 5.

Appearance and existence of characteristic electronic z oscillations at frequencies $\omega_z^{\rm osc}$ in $H_2{}^+$ and HD^+ can be explained on the basis of the following:

(i) the concept of nuclear continuum states Ψ_C which are prepared by the laser pulses and have the energies $E_C = E_0 + \omega_z^{\rm osc}$, where E_0 are the energies of initial states ψ_0;

(ii) the fact that the majority of $H_2{}^+$ and HD^+ ions returns back to their initial states ψ_0 after the ends of the laser pulses (the respective probability ranges from 0.61 to 0.73 in our present simulations);

(iii) the fact of formation of vibrationally cold and hot ensembles of $H_2{}^+$ and HD^+, as described above [Figs. 3(c)–3(e)] and in Ref. [11].

While the first issue listed above is the assumption advanced in our previous works [11,12] for the $H_2{}^+$ ion excited just *below* its dissociation threshold, the other two issues are based on our numerical simulations of the non-Born-Oppenheimer quantum dynamics of $H_2{}^+$ and HD^+ in the present and previous [11,12] works. Moreover, formation of vibrationally cold and hot ensembles of SF_6 and CF_3I molecules was observed experimentally [19].

The overall process, where $H_2{}^+$ or HD^+ is involved in, can be described as follows. The molecular ion at hand is excited from its ground state ψ_0 by a strong and short one-cycle laser pulse chosen such that the energy of the ion by the end of the pulse $\langle E(t_p)\rangle$ is above its dissociation threshold. During the laser pulse, the energy of the ion can be substantially higher than $\langle E(t_p)\rangle$ [see, e.g., Figs. 2(a) and 2(d)]. At the same time, there is a significant probability to return back to the initial ground state ψ_0 (as specified in the second issue

above). Therefore, two ensembles (vibrationally hot and cold) are formed, as shown in Figs. 3(c)–3(e). The hot ensemble is represented by the nuclear continuum state Ψ_C, while the cold ensemble for the most part by the initial state ψ_0. Since there is a significant energy gap between the two states $E_C - E_0 = \omega_z^{\rm osc}$, and the final state of the ion prepared by the laser pulse is by no means an eigenstate, coherent oscillations (quantum beats) at the carrier frequency $\omega_z^{\rm osc}$ appear after the end of the pulse and manifest themselves as smoothly shaped electronic oscillations in the symmetric homonuclear H_2^+ ion (Fig. 4), or as time-delayed "echo pulses" in the asymmetric heteronuclear HD^+ ion (Fig. 5).

We note that formation of hot and cold ensembles implies that the energies of continuum states Ψ_C of H_2^+ and HD^+, prepared by the laser pulses, should be higher than their energies at the ends of the laser pulses, $\langle E(t_p)\rangle$, and it is easy to check that this is really the case. Indeed, in the case of H_2^+, $E_0 = -0.597\,14$ a.u. and $\omega_z^{\rm osc} = 0.220\,37$ a.u., while in the case of HD^+, $E_0 = -0.597\,89$ a.u. and $\omega_z^{\rm osc} = 0.235\,57$ a.u. Therefore, the energies of continuum states Ψ_C, prepared by the laser pulses, are as follows: $E_C^{H_2^+} = -0.376\,77$ a.u. and $E_C^{HD^+} = -0.362\,32$ a.u.. The possibility to prepare continuum states Ψ_C with similar energies by one-cycle laser pulses at $\lambda_l = 400$ and 50 nm was analyzed in more detail previously [12].

We should also notice that a lot of interesting phenomena induced by linearly polarized laser pulses are initiated by the release of an electron from the parent molecule or molecular ion, as explained by the recollision model of Corkum [1] and electron-field following. In particular, it was shown that multiple ionization bursts may occur in H_2^+ along the polarization direction (z) of an intense infrared laser field [24]. Similar phenomena were reported previously to exist for both laser-driven z and transversal ρ degrees of freedom of H_2^+ and HD^+ [3,4]. Nowadays, strong-field photoelectron holography is a hot topic for time-resolved imaging of electrons in molecules [25]. The holographic interference of a direct (reference) electron wave with backward rescattered one (signal) has been proposed in Ref. [26] as a sensitive probe of molecular structure. Transversal ρ distribution of electronic density was not studied in Refs. [24–26]. We believe that accounting for transversal electronic motion, which is always excited due to the wave properties of an electron, could enrich the overall picture of photoelectron holography [25]. Excitation and the post-laser-pulse free evolution of the optically passive transversal ρ degree of freedom of an electron in H_2^+ and HD^+ will be analyzed in the next section.

V. ELECTRONIC ρ OSCILLATIONS, INTERNUCLEAR DISTANCE, AND ACCELERATION

Since the transversal ρ degree of freedom of the electron is optically passive, its motion is excited only due to electronic z oscillations induced by the laser field and the wave properties of the electron. Electronic ρ oscillations thus appear in H_2^+ and HD^+, which are presented in Fig. 6 (left and right panel, respectively). Similarly to "z oscillations" discussed above, the term "ρ oscillations" is used below to describe oscillations of both expectation values $\langle\rho\rangle$ and accelerations $d^2\langle\rho\rangle/dt^2 = m_{\rm e}^{-1}\langle -\partial V/\partial\rho\rangle$, where $m_{\rm e} = 1$ a.u.

In Figs. 6(a) and 6(d), time-dependent expectation values $\langle\rho\rangle$ are shown together with internuclear distances $\langle R\rangle$ in the case when the laser wavelength is $\lambda_l = 50$ nm. It is easy to see that local minima of internuclear distances (e.g., at $t \approx 120$ fs in H_2^+ and at $t \approx 160$ fs in HD^+) correlate with the maximal amplitudes of respective ρ oscillations. The reason is similar to that of electronic z oscillations discussed in the previous section. Indeed, when nuclei come close to each other and the bond length $\langle R\rangle$ decreases, the component of the Coulomb force along the transversal ρ degree of freedom increases and the amplitude of electronic ρ oscillations rises accordingly. On the other hand, at a large amplitude of ρ oscillations, the electron becomes more delocalized and electron density between the nuclei decreases. Therefore, Coulombic repulsion of two nuclei acts more efficiently and causes the bond length to change from contraction to elongation.

In Figs. 6(b) and 6(e), electronic ρ oscillations in H_2^+ and HD^+ are presented by time-dependent expectation values $\langle -\partial V/\partial\rho\rangle$, i.e., accelerations, at the laser wavelength $\lambda_l = 50$ nm. It is seen from the comparison of Figs. 6(b) and 4(b) and 4(d) that in homonuclear H_2^+, electronic ρ oscillations are quite different from z oscillations. While expectation values $\langle -\partial V/\partial z\rangle$ appear for H_2^+ in Figs. 4(b) and 4(d) as regular fast oscillations temporally shaped with the period $\tau_{\rm shp} \approx 30$ fs, expectation values $\langle -\partial V/\partial\rho\rangle$ shown in Fig. 6(b) first demonstrate slow oscillations with the period $\tau_{\rm shp} \approx 30$ fs, which are modulated with fast small-amplitude oscillations, followed by an "echo pulse" of fast oscillations at around $t \approx 120$ fs. In contrast, in heteronuclear HD^+, electronic ρ oscillations [Fig. 6(e)] are quite similar to z oscillations [Fig. 5(d)]. Indeed, in both cases we see "echo pulses" appearing at around $t \approx 80$ fs and $t \approx 160$ fs. In general, two main characteristic frequencies of fast ρ oscillations in H_2^+ and HD^+ can be distinguished at a close look at Figs. 6(a), 6(b), 6(d), and 6(e), as detailed in Figs. 6(c) and 6(f).

Time-dependent expectation values $\langle -\partial V/\partial\rho\rangle$, presented in Fig. 6(c) for H_2^+ excited at $\lambda_l = 50$ and 400 nm (indicated near the curves), demonstrate at about $t \approx 80$ fs a rather abrupt transition from the oscillation frequency of $\omega_{\partial V/\partial\rho}^{\rm osc(1)} \approx \omega_z^{\rm osc}$ to $\omega_{\partial V/\partial\rho}^{\rm osc(2)} \approx 2\omega_z^{\rm osc}$, as it was expected due to the discussed above effect of frequency doubling of electronic ρ oscillations with respect to its z oscillations [11,12]. In contrast, in Fig. 6(f), where time-dependent expectation values $\langle -\partial V/\partial\rho\rangle$ of HD^+ are presented, we can clearly see the opposite behavior, an abrupt transition from the higher oscillation frequency $\omega_{\partial V/\partial\rho}^{\rm osc(2)} \approx 2\omega_z^{\rm osc}$ to the lower one $\omega_{\partial V/\partial\rho}^{\rm osc(1)} \approx \omega_z^{\rm osc}$, occurring at about $t \approx 150$ fs. We can assume, therefore, that power spectra of electronic ρ oscillations in H_2^+ and HD^+ may contain both the second and the fourth *higher-order* harmonics of the laser carrier frequency ω_l at $\lambda_l = 400$ nm, as well as the fourth and the second *lower-order* harmonics at $\lambda_l = 50$ nm.

As it was discussed earlier, nuclear motion manifests itself in the post-laser-pulse electronic oscillations in two ways. On the one hand, local minima of the internuclear distance $\langle R\rangle$ correspond to the domains of large-amplitude electronic z oscillations (Fig. 5) and electronic ρ oscillations (Fig. 6), while local maxima of $\langle R\rangle$ correspond to rather small amplitudes of

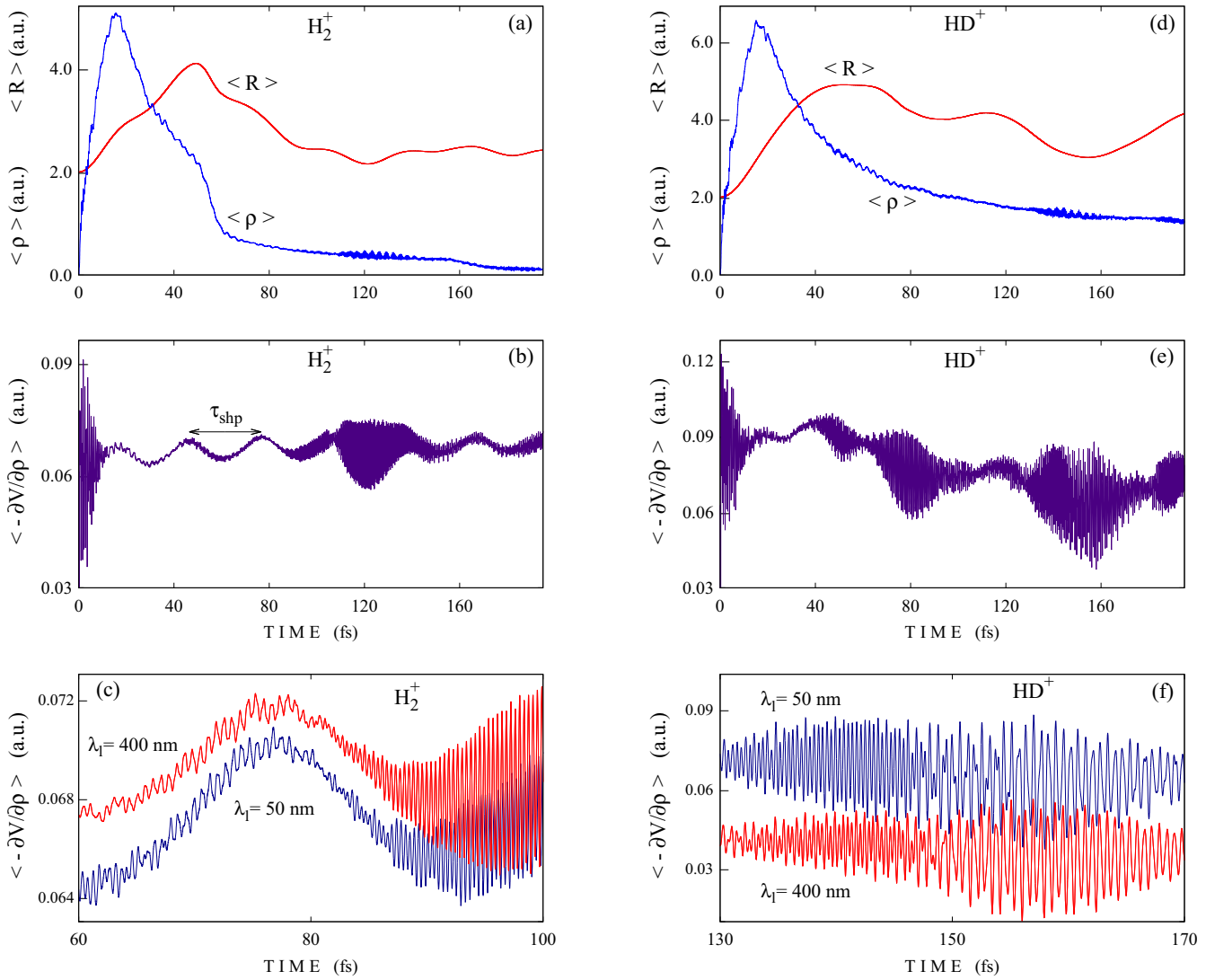

FIG. 6. Electronic ρ oscillations in $H_2{}^+$ (left panel) and HD^+ (right panel): (a), (d) time-dependent expectation values $\langle R\rangle$ and $\langle\rho\rangle$ at $\lambda_l = 50$ nm; (b), (e) time-dependent expectation values $\langle -\partial V/\partial\rho\rangle$ at $\lambda_l = 50$ nm; (c), (f) time-dependent expectation values $\langle -\partial V/\partial\rho\rangle$ at $\lambda_l = 50$ and 400 nm on shorter timescales.

electronic oscillations. On the other hand, temporal shaping of electronic z oscillations in $H_2{}^+$ (Fig. 4) is also caused by nuclear motion [11,12]. Both features can be easily described in terms of nuclear acceleration $d^2\langle R\rangle/dt^2$ as follows.

From Ehrenfest's theorem, the acceleration of expectation value $\langle R\rangle$, i.e., the nuclear acceleration, reads as

$$\frac{d^2\langle R\rangle}{dt^2} = -\frac{1}{m_\mathrm{n}}\left\langle\frac{\partial}{\partial R}[V - \mathcal{E}(t)d_z]\right\rangle, \tag{11}$$

where m_n is the nuclear reduced mass, V is the Coulomb potential given by Eq. (4), $\mathcal{E}(t)$ is the laser electric field, and d_z is the component of the dipole moment along the z axis given by Eq. (1) or (2). In the case of heteronuclear HD^+, the nuclear acceleration

$$\frac{d^2\langle R\rangle}{dt^2} = -\frac{1}{m_\mathrm{n}}\left[\left\langle\frac{\partial V}{\partial R}\right\rangle + e\,\mathcal{E}(t)\frac{M_\mathrm{d} - M_\mathrm{p}}{M_\mathrm{d} + M_\mathrm{p}}\right], \tag{12}$$

where e is the electron charge, M_d and M_p are the deuteron and proton masses, whereas in the case of homonuclear $H_2{}^+$, d_z is independent of R and the nuclear acceleration depends on the Coulomb potential only.

As it has been concluded from the previous discussion, there are two characteristic times of post-laser-pulse electronic z and ρ oscillations which are related to nuclear motion:

(i) temporal shaping of z oscillations in $H_2{}^+$ with the period of $\tau_\mathrm{shp} \approx 30$ fs (Fig. 4) and the existence of ρ oscillations in $H_2{}^+$ with the same period [Fig. 6(b)], i.e., pure coherence;

(ii) the appearance of "echo pulses" in HD^+ with the period of $\tau_\mathrm{echo} \approx 80$ fs [see Fig. 5 for z oscillations and Fig. 6(e) for ρ oscillations].

The frequencies of nuclear oscillations, which correspond to the periods of $\tau_\mathrm{shp} \approx 30$ fs and $\tau_\mathrm{echo} \approx 80$ fs, are $\omega_\mathrm{shp} \approx 0.506\,61 \times 10^{-2}$ a.u. and $\omega_\mathrm{echo} \approx 0.189\,98 \times 10^{-2}$ a.u., respectively. Note that the frequencies ω_{01} of the $|v = 0\rangle \rightarrow |v = 1\rangle$ vibrational transitions in $H_2{}^+$ and HD^+ are $0.998\,34 \times 10^{-2}$ a.u. and $0.871\,61 \times 10^{-2}$ a.u., respectively [27]. Therefore, both ω_shp and ω_echo correspond to the so-

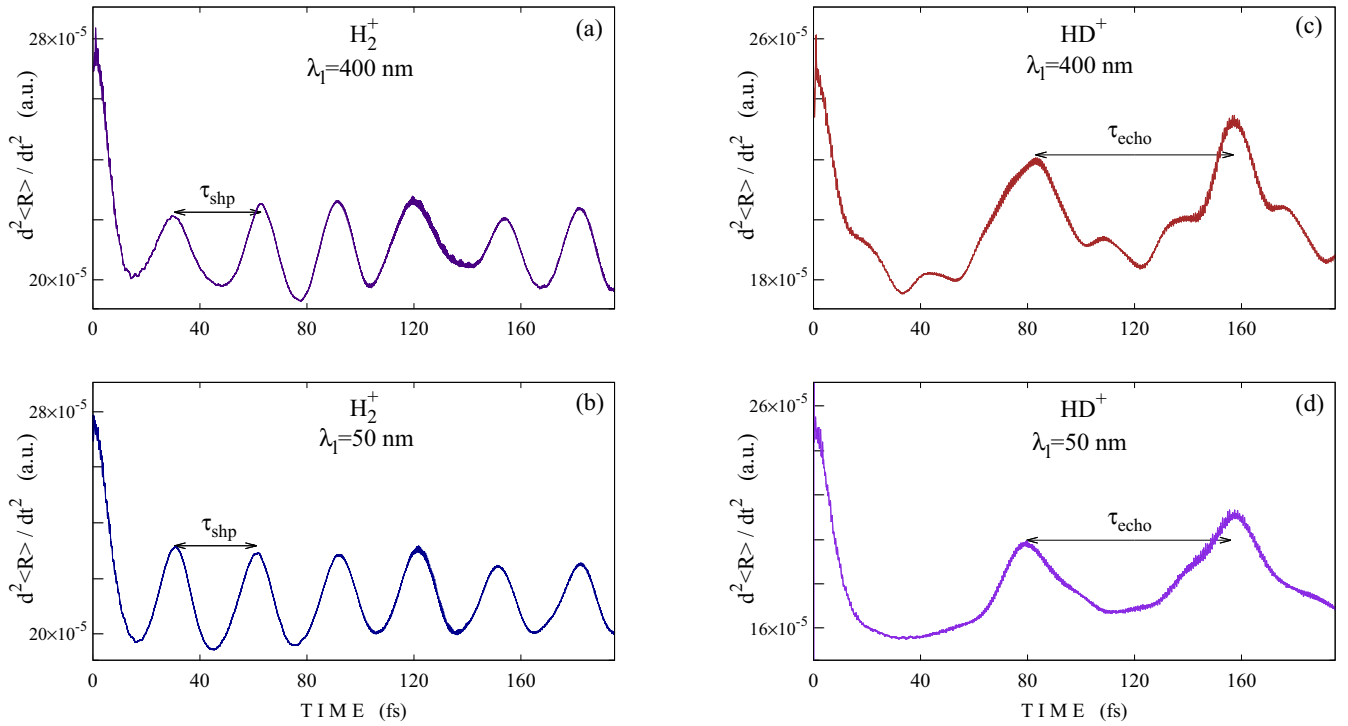

FIG. 7. Nuclear acceleration in H_2^+ (left panel) and HD^+ (right panel): time-dependent expectation values $d^2\langle R\rangle/dt^2$ at the laser wavelength $\lambda_l = 400$ nm (top) and $\lambda_l = 50$ nm (bottom).

called *under-resonant* [4] or *below-resonant* [28] frequencies, $\omega < \omega_{01}$, which can provide very efficient vibrational excitation of H_2^+ and HD^+, being used as the laser carrier frequency ω_l. The case of $\omega_l \approx \omega_{01}/2$ (i.e., $\omega_l \approx \omega_{shp}$) has been already studied [4,28], while the case of $\omega_l \approx \omega_{echo}$ will be addressed in our future work. It is interesting to see, therefore, how the above-specified *below-resonant* frequencies ω_{shp} and ω_{echo} are related to nuclear accelerations $d^2\langle R\rangle/dt^2$ in H_2^+ and HD^+.

In Fig. 7, nuclear accelerations $d^2\langle R\rangle/dt^2$ in H_2^+ and HD^+ are presented at the laser wavelength $\lambda_l = 400$ nm [Figs. 7(a) and 7(c)] and $\lambda_l = 50$ nm [Figs. 7(b) and 7(d)]. First of all, we notice a substantial difference of nuclear accelerations in H_2^+ (left panel) and in HD^+ (right panel) at both laser wavelengths used. Indeed, in homonuclear H_2^+ [Figs. 7(a) and 7(b)], nuclear accelerations at $\lambda_l = 400$ nm and at $\lambda_l = 50$ nm are quite similar to each other. In both cases, they appear as rather regular oscillations with the period of $\tau_{shp} \approx 30$ fs, corresponding to the period of envelope modulation of electronic z oscillations in H_2^+ (Fig. 4). The frequency of nuclear oscillations in H_2^+ corresponding to $\tau_{shp} \approx 30$ fs is $\omega_{shp} \approx 0.506\,61 \times 10^{-2}$ a.u. (1111.8803 cm^{-1}). In the case of $\lambda_l = 400$ nm ($\omega_l = 0.113\,91$ a.u.), the ratio ω_{shp}/ω_l is about 0.0445, which approximately corresponds to the 22nd *lower-order* harmonic of ω_l. In the case of $\lambda_l = 50$ nm ($\omega_l = 0.911\,27$ a.u.), the ratio ω_{shp}/ω_l is only about 0.005 56 and approximately corresponds to the 180th *lower-order* harmonic of ω_l. In contrast, in heteronuclear HD^+ [Figs. 7(c) and 7(d)], regular oscillations of $d^2\langle R\rangle/dt^2$ with the period of $\tau_{shp} \approx 30$ fs do not appear at all. Instead, comparatively slow large-amplitude oscillations with the period $\tau_{echo} \approx 80$ fs are dominant. They correspond to the appearance of "echo pulses" of electronic z oscillations (Fig. 5) and ρ oscillations [Fig. 6(e)]. Nuclear oscillations with the period of $\tau_{sat} \approx 20$ fs and comparatively small amplitude appear only in the case of $\lambda_l = 400$ nm, as "satellites" of dominant "echo pulses," around $t \approx 40$ fs, $t \approx 120$ fs, and $t \approx 180$ fs [Fig. 7(c)]. The period $\tau_{echo} \approx 80$ fs corresponds to the frequency of $\omega_{echo} \approx 0.189\,98 \times 10^{-2}$ a.u. (416.9579 cm^{-1}), while the period $\tau_{sat} \approx 20$ fs corresponds to the frequency $\omega_{sat} \approx 0.759\,92 \times 10^{-2}$ a.u. (1667.8315 cm^{-1}). In the case of $\lambda_l = 400$ nm, the ratio ω_{echo}/ω_l is about 0.016 68, which is close to the 60th *lower-order* harmonic of ω_l, while the ratio ω_{sat}/ω_l is about 0.066 71 and corresponds to the 15th *lower-order* harmonic. In the case of $\lambda_l = 50$ nm, the ratio ω_{echo}/ω_l is only $0.208\,48 \times 10^{-2}$, which approximately corresponds to the 480th *lower-order* harmonic of ω_l.

We can conclude, therefore, that very low harmonics are to be expected to appear in the power spectra related to nuclear motion in H_2^+ and HD^+. On the other hand, it is clearly seen from Fig. 7 that all large-amplitude oscillations of $d^2\langle R\rangle/dt^2$ are modulated with small-amplitude fast oscillations. Since the amplitudes of these fast oscillations are very small indeed, only weak *higher-order* harmonics can be expected.

VI. POWER SPECTRA OF ELECTRONIC AND NUCLEAR MOTION IN H_2^+ AND HD^+

In this section we present power spectra generated by electronic degrees of freedom z, ρ and by the nuclear degree of freedom R in H_2^+ and HD^+ calculated in the acceleration form. All power spectra are presented below as functions of frequency ω in units of the laser carrier frequency ω_l and the laser field is taken into account where appropriate.

The characteristic feature of power spectra generated by electronic degrees of freedom of H_2^+ excited slightly be-

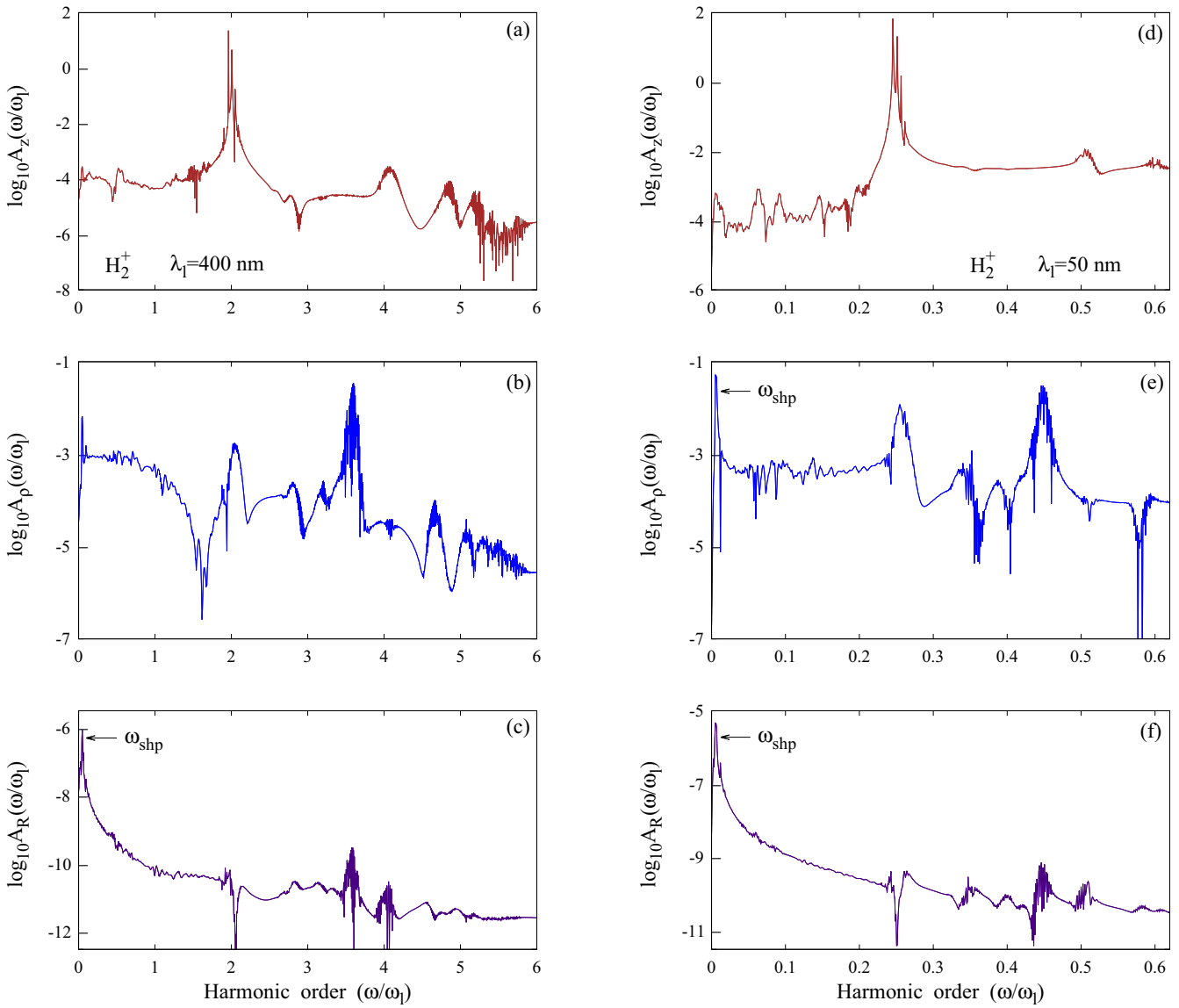

FIG. 8. Power spectra $A_z(\omega)$, $A_\rho(\omega)$, and $A_R(\omega)$ of $H_2{}^+$ excited at the wavelength $\lambda_l = 400$ nm (left panel) and $\lambda_l = 50$ nm (right panel).

low the dissociation threshold by one- and two-cycle laser pulses [11,12] is a small number of generated harmonics. Specifically, not more than three relatively strong harmonics were observed in power spectra calculated in Refs. [11,12]. In Fig. 8, power spectra $A_z(\omega)$, $A_\rho(\omega)$, and $A_R(\omega)$ generated by z, ρ, and R degrees of freedom of $H_2{}^+$ excited above the dissociation threshold by one-cycle laser pulses at $\lambda_l = 400$ nm (left panel) and $\lambda_l = 50$ nm (right panel) are presented.

In power spectra $A_z(\omega)$ generated by the optically active z degree of freedom of the electron [Figs. 8(a) and 8(d)], we note a strong second *higher-order* harmonic at $\lambda_l = 400$ nm [Fig. 8(a)] and a strong fourth *lower-order* harmonic at $\lambda_l = 50$ nm [Fig. 8(d)]. The appearance of both aforementioned harmonics was expected from our previous analysis of post-laser-pulse electronic z oscillations (see Fig. 4 and related discussion in the text). Both harmonics contain, in particular, the characteristic frequency of electronic z oscillations, $\omega_z^{\rm osc} = 0.220\,37$ a.u., close to their maxima. All other harmonics are comparatively very weak, although the lowest harmonics are well pronounced, especially those generated at $\lambda_l = 50$ nm [Fig. 8(d)].

Power spectra $A_\rho(\omega)$ of the transversal ρ degree of freedom of $H_2{}^+$ [Figs. 8(b) and 8(e)] provide a clear illustration of the discussed earlier effect of frequency doubling of electronic ρ oscillations [11,12]. Indeed, both the second *higher-order* harmonic at $\lambda_l = 400$ nm [Fig. 8(b)] and the fourth *lower-order* harmonic at $\lambda_l = 50$ nm [Fig. 8(e)] well correspond to the characteristic frequency $\omega_\rho^{(1)} \approx \omega_z^{\rm osc}$, while each of two higher harmonics in both cases corresponds to the doubled frequency $\omega_\rho^{(2)} \approx 2\omega_z^{\rm osc}$. A rather sharp transition from $\omega_\rho^{(1)}$ to $\omega_\rho^{(2)}$ during post-laser-pulse free evolution of $H_2{}^+$ at about $t \approx 80$ fs was illustrated in Fig. 6(c). Note finally that the lowest harmonics of all power spectra of electronic motion [Figs. 8(a), 8(b), 8(d), and 8(e)] correspond to the frequency of $\omega_{\rm shp} \approx 0.506\,61 \times 10^{-2}$ a.u. (1111.8803 cm^{-1}) defined in the previous section from the period of $\tau_{\rm shp} \approx 30$ fs [Figs. 7(a) and 7(b)], as explicitly indicated in Fig. 8(e), where this harmonic is even stronger than the others.

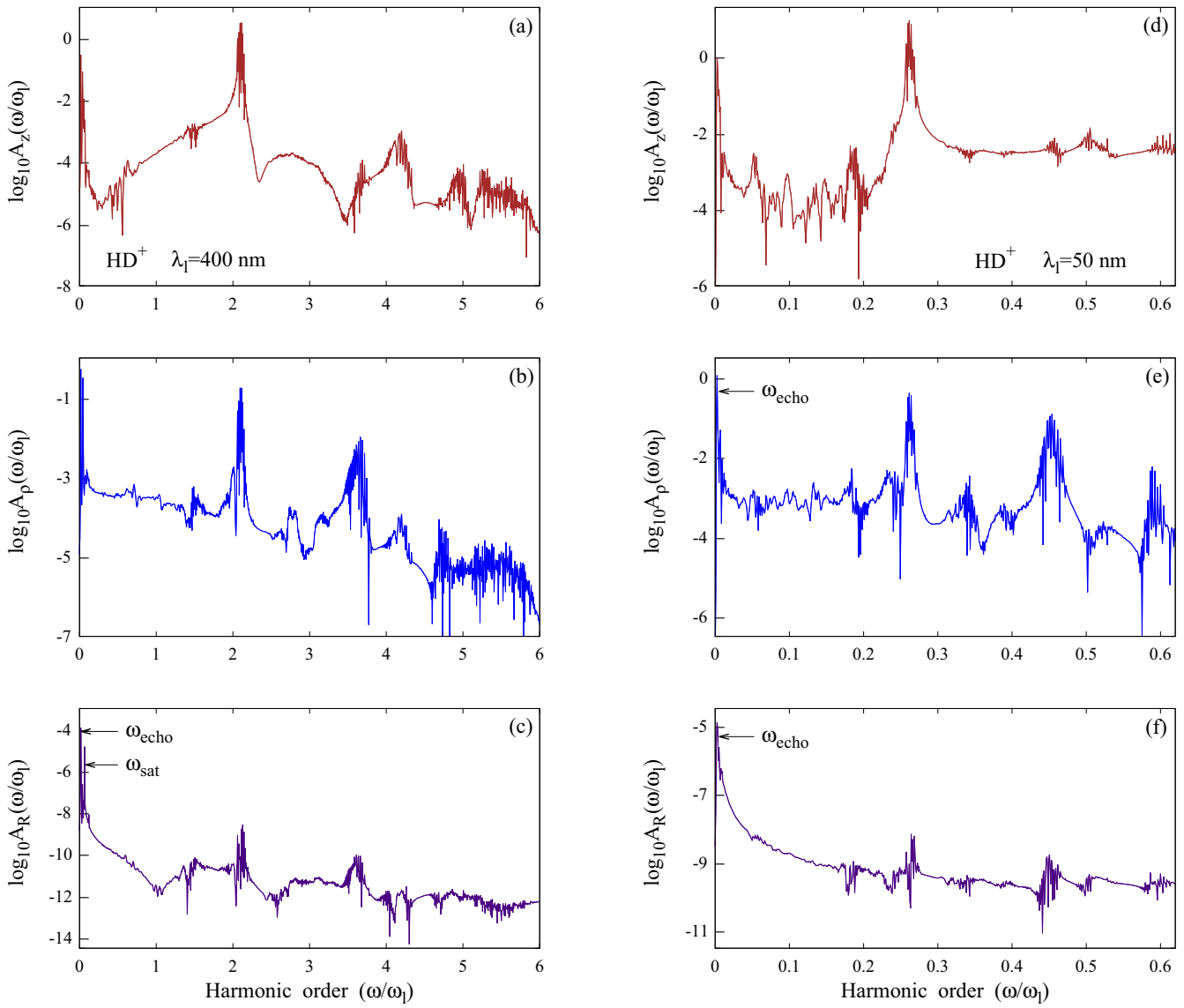

FIG. 9. Power spectra $A_z(\omega)$, $A_\rho(\omega)$, and $A_R(\omega)$ of HD^+ excited at the wavelength $\lambda_l = 400$ nm (left panel) and $\lambda_l = 50$ nm (right panel).

In power spectra $A_R(\omega)$ related to nuclear motion [Figs. 8(c) and 8(f)], the strongest harmonics indeed correspond to the frequency $\omega_{\rm shp}$, as it was expected from the time-dependent nuclear acceleration $d^2\langle R\rangle/dt^2$ presented in Figs. 7(a) and 7(b), while higher harmonics are much weaker. An interesting feature of nuclear power spectra $A_R(\omega)$ presented in Figs. 8(c) and 8(f) is the existence of deep and rather wide minima at $\omega/\omega_l \approx 2$ ($\lambda_l = 400$ nm) and at $\omega/\omega_l \approx 0.25$ ($\lambda_l = 50$ nm) corresponding to respective maxima of $A_\rho(\omega)$ at $\omega \approx \omega_\rho^{(1)}$ [Figs. 8(b) and 8(e)]. This feature can be explained by the interaction of nuclear and electronic motion as follows. On the one hand, a deep minimum in the $A_R(\omega)$ spectrum indicates a very small kinetic energy of nuclear motion, which may correspond, e.g., to one of the classical turning points. On the other hand, a strong maximum of the respective $A_\rho(\omega)$ spectrum at $\omega \approx \omega_\rho^{(1)}$ indicates a large kinetic energy of electronic ρ oscillations, which corresponds to a small internuclear distance when the component of the Coulomb force along the ρ axis is large. We can assume, therefore, that deep and wide minima of power spectra $A_R(\omega)$ at $\omega \approx \omega_\rho^{(1)}$ [Figs. 8(c) and 8(f)] correspond to inner turning points of nuclear motion. Advanced above physical mechanism, that explains the correspondence of strong minima of $A_R(\omega)$ spectra to maxima of $A_\rho(\omega)$ spectra, is especially efficient in homonuclear systems, where two identical nuclei perform a "symmetric" motion, always being at the same distances from their center of mass, on the one hand, and from the maximum of electronic density, on the other hand. This symmetry of nuclear motion is definitely broken in heteronuclear systems, and we can expect, therefore, a much less pronounced similar effect to appear in power spectra of HD^+ (see Fig. 9 below).

Power spectra of electronic and nuclear motion in HD^+ excited above the dissociation threshold by one-cycle laser pulses at $\lambda_l = 400$ nm (left panel) and at $\lambda_l = 50$ nm (right panel) are presented in Fig. 9. Although in heteronuclear HD^+, the nuclear degree of freedom R is optically active small dipole, it is seen from the comparison of Figs. 9 and 8 that

power spectra of HD^+ are very similar to those of $H_2{}^+$, which can be explained by a very short duration of the laser pulses used in both cases. For example, power spectra $A_z(\omega)$ of $H_2{}^+$ and HD^+ excited at $\lambda_l = 400$ nm [Figs. 8(a) and 9(a), respectively] have strong and sharp second *higher-order* harmonics at $\lambda \approx 200$ nm, while their fourth *higher-order* harmonics at $\lambda \approx 100$ nm are comparatively weak and have rather complicated structure, especially in the case of HD^+ [Fig. 9(a)]. This effect can be explained by frequency modulation of intercycle dynamics in molecular high-order harmonic generation [6]. Nevertheless, some distinctive features of power spectra of $H_2{}^+$ and HD^+ should be noticed.

First of all, we note that the lowest harmonics of electronic power spectra $A_z(\omega)$ of $H_2{}^+$ [Figs. 8(a) and 8(d)] are by about two orders of magnitude stronger than those of HD^+ [Figs. 9(a) and 9(d)]. This difference is much less pronounced in electronic power spectra $A_\rho(\omega)$, although at $\lambda_l = 400$ nm [Fig. 9(b)], the lowest harmonic in HD^+ is even stronger than any other one, in contrast to $H_2{}^+$ [Fig. 8(b)]. It is clearly seen from Figs. 9(c) and 9(f) that minima in nuclear power spectra $A_R(\omega)$ of HD^+ at $\omega/\omega_l \approx 2$ ($\lambda_l = 400$ nm) and at $\omega/\omega_l \approx 0.25$ ($\lambda_l = 50$ nm) are much less pronounced than those in power spectra of $H_2{}^+$ [Figs. 8(c) and 8(f)], as it was already expected on the basis of "asymmetry" of nuclear motion in heteronuclear systems. Finally, in power spectra $A_R(\omega)$ related to nuclear motion in HD^+ [Figs. 9(c) and 9(f)], the strongest low harmonics correspond not to the frequency $\omega_{\rm shp}$ related to $H_2{}^+$ [Figs. 8(c) and 8(f)], but to the frequency of $\omega_{\rm echo}$, as it was expected from the time-dependent nuclear acceleration $d^2\langle R\rangle/dt^2$ [Figs. 7(c) and 7(d)]. Also, note that at $\lambda_l = 400$ nm, a low harmonic corresponding to the frequency $\omega_{\rm sat}$, defined in the previous section as the frequency of "satellite" oscillations near the dominant "echo pulses" of nuclear acceleration [Fig. 7(c)], is also well pronounced, as explicitly indicated in Fig. 9(c).

VII. CONCEPT OF INVERSION SYMMETRY OF ELECTRONIC MOTION AND AN ALTERNATIVE NOMENCLATURE FOR THE HARMONIC ORDER

According to the concept of inversion symmetry for electronic motion in diatomic molecules, discussed, e.g., in Ref. [5], power spectra generated by optically active (z) degrees of freedom of electrons of homonuclear molecules may contain only odd harmonics, while both odd and even harmonics can be generated by heteronuclear molecules. In particular, the non-Born-Oppenheimer simulations, performed in Ref. [5], showed that only odd harmonics were generated by the H_2 molecule, while both odd and even harmonics were generated by the HD molecule. These results were explained on the basis of the concept of inversion symmetry for electronic motion as follows. In homonuclear H_2, laser-driven electrons always perform "symmetric" oscillations consisting of only odd frequency components [5], while in heteronuclear HD, where the center of nuclear masses is different from the center of nuclear charges, the symmetry of electronic oscillations is broken, which results in the generation of even harmonics as well. Similar results were obtained in our previous work [10] for muonic molecular ions: only odd harmonics were generated by the optically active z degree of freedom of the laser-driven muon in homonuclear $dd\mu$, while both odd and even harmonics were generated by heteronuclear $dt\mu$.

In both Refs. [5,10], shaped laser pulses used for the excitation of a system at hand contained more than a dozen of optical cycles, and the results obtained for power spectra of the laser-driven z degrees of freedom of bound particles (electrons or muons) were in a full agreement with the concept of inversion symmetry for electronic or muonic motion. In contrast, in this study we consider the case of short one-cycle laser pulses used for the initial excitation of a system under consideration, while the power spectra are generated mainly during its post-laser-pulse free evolution. At a first glance, the resulting power spectra $A_z(\omega)$ of both $H_2{}^+$ and HD^+ presented in Figs. 8(a) and 8(d), and in Figs. 9(a) and 9(d), respectively, are in a disagreement with the concept of inversion symmetry for electronic motion [5]. Indeed, only even harmonics appear at $\lambda_l = 400$ nm and only *lower-order* harmonics appear in the case of $\lambda_l = 50$ nm. It is interesting, therefore, whether such an agreement can be found.

The gap can be bridged by introducing an alternative, rationalized definition for the harmonic order, similar to that tested in our previous work [12] for $H_2{}^+$. Indeed, in the case of a long laser pulse, that is linearly polarized along the z axis and contains many optical cycles, the laser-driven molecular electron performs z oscillations with the frequency equal to the laser carrier frequency ω_l due to the adiabatic electron-field following. Therefore, the commonly used definition of the harmonic order as ω/ω_l implies, in fact, that the frequency ω in power spectra $A(\omega)$ is measured in units of the frequency of electronic z oscillations. In contrast, when a very short one-cycle laser pulse is used for the initial excitation only, the subsequent post-laser-pulse electronic z oscillations occur with the characteristic frequency $\omega_z^{\rm osc}$ which, in a general case, *is not* equal to the laser carrier frequency ω_l. In the latter case, therefore, it is reasonable to measure the frequency in units of $\omega_z^{\rm osc}$ and define thus rationalized harmonic order as $\omega/\omega_z^{\rm osc}$. Recall that characteristic frequencies $\omega_z^{\rm osc}$, occurring in $H_2{}^+$ and HD^+, are different: $\omega_z^{\rm osc} = 0.220\,37$ a.u. in $H_2{}^+$ and $\omega_z^{\rm osc} = 0.235\,57$ a.u. in HD^+.

In Fig. 10, power spectra generated by electronic and nuclear motion in $H_2{}^+$ at $\lambda_l = 50$ nm and in HD^+ at $\lambda_l = 400$ nm are presented in terms of the rationalized harmonic order $\omega/\omega_z^{\rm osc}$. It is clearly seen from the comparison of power spectrum of electronic z oscillations in $H_2{}^+$ excited at $\lambda_l = 50$ nm [Fig. 10(a)] to that of Fig. 8(d), as well as the power spectrum of HD^+ excited at $\lambda_l = 400$ nm [Fig. 10(d)] to that presented in Fig. 9(a), that power spectra $A_z(\omega/\omega_z^{\rm osc})$ are in a good agreement with the concept of inversion symmetry for electronic motion in homonuclear and heteronuclear diatomic molecules [5]. It is also seen from Figs. 10(b), 10(c), 10(e), and 10(f) that rationalized harmonic order $\omega/\omega_z^{\rm osc}$ is suitable for the presentation of power spectra $A_\rho(\omega/\omega_z^{\rm osc})$ and $A_R(\omega/\omega_z^{\rm osc})$ as well.

Note, finally, that a common harmonic order used in Figs. 8 and 9 and the rationalized harmonic order used in Fig. 10 are, in fact, equivalent to each other since, in both cases, harmonic frequency ω is measured in terms of the frequency of electronic z oscillations, as it was discussed in this section earlier.

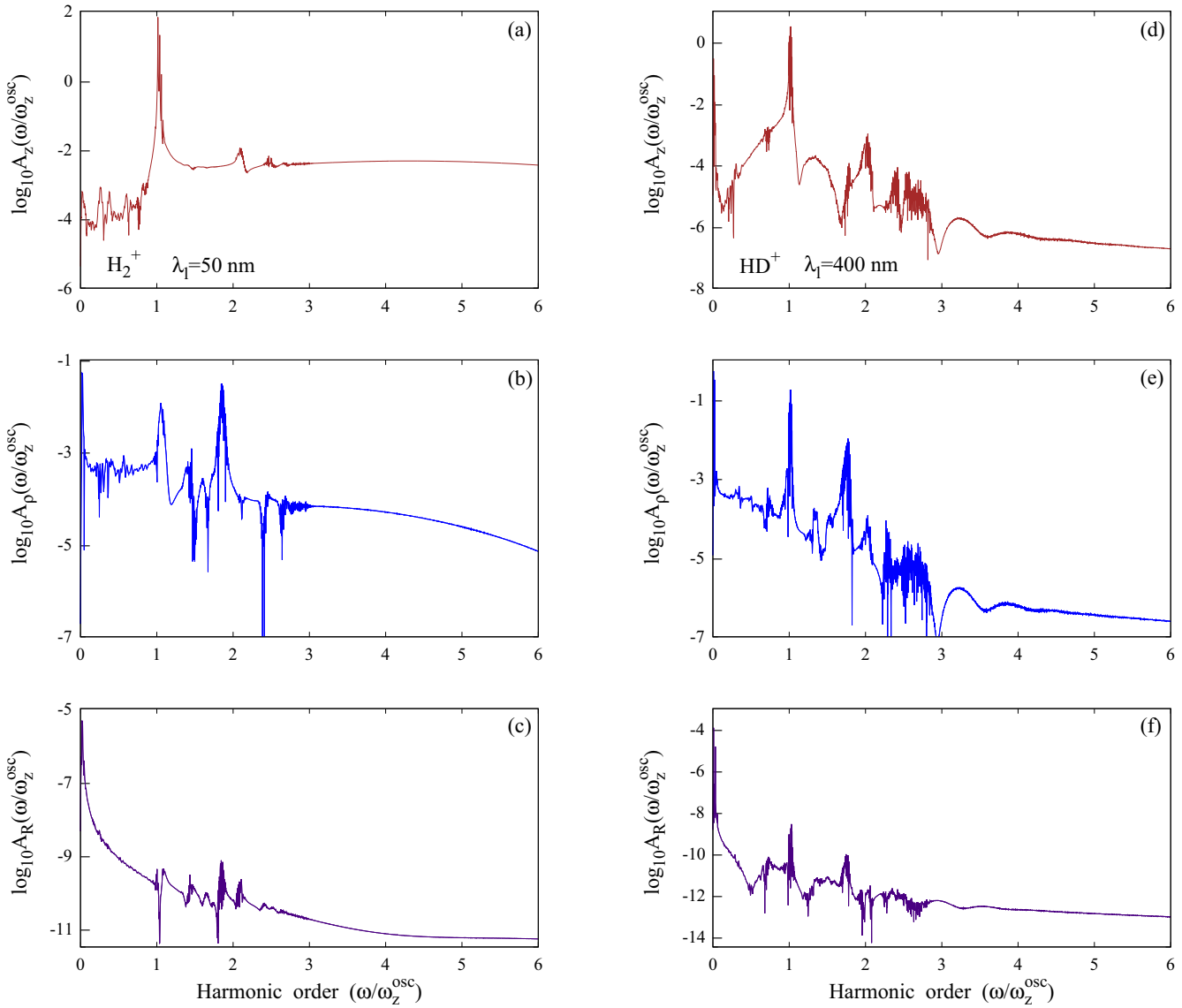

FIG. 10. Power spectra of H_2^+ excited at the wavelength $\lambda_l = 50$ nm (left panel) and power spectra of HD^+ excited at $\lambda_l = 400$ nm (right panel) in terms of the rationalized harmonic order ω/ω_z^{osc}.

VIII. CONCLUSION

In this work, we have studied numerically the non-Born-Oppenheimer quantum dynamics and long-term post-laser-pulse free evolution of homonuclear H_2^+ and its heteronuclear isotope HD^+, both being excited to the nuclear continuum by strong and short one-cycle laser pulses at the wavelengths of $\lambda_l = 400$ and 50 nm. Power spectra of both electronic and nuclear motion have been calculated. Our main objectives can be clarified as follows.

(1) One-cycle laser pulses have been used because they result in only one recollision of the laser-driven electron with nuclei. They provide, therefore, a limiting case for the recollision model of Corkum [1] and may give rise to a different, new mechanism of the generation of other harmonics.

(2) The choice of the laser wavelengths was based on our previous works [11,12] and has made it possible to study the generation of both *higher*-order harmonics at $\lambda_l = 400$ nm and *lower*-order harmonics at $\lambda_l = 50$ nm, calculated in terms of the laser carrier frequency ω_l.

(3) The use of strong laser pulses, enabling to excite H_2^+ and HD^+ above the dissociation threshold, has made it possible to evaluate the influence of a significant bond elongation and dissociation on the characteristic frequencies of post-laser-pulse electronic z and ρ oscillations.

(4) The study of both homonuclear H_2^+ and heteronuclear HD^+ has made it possible to compare their electronic power spectra $A_z(\omega/\omega_l)$ on the basis of the concept of inversion symmetry for diatomic molecules [5] and suggest a rationalized harmonic order in terms of the characteristic frequency ω_z^{osc} of post-laser-pulse electronic z oscillations.

The following conclusions can be made from the results of this work.

Excitation of H_2^+ and HD^+ by short one-cycle laser pulses gives rise to post-laser-pulse electronic z and ρ oscillations, occurring with the frequencies different from the laser carrier

frequency ω_l. There are three frequencies of post-laser-pulse electronic oscillations: (i) characteristic frequency $\omega_z^{\rm osc}$ of the laser-induced electronic z oscillations and (ii) two frequencies $\omega_\rho^{(1)} \approx \omega_z^{\rm osc}$ and $\omega_\rho^{(2)} \approx 2\omega_z^{\rm osc}$ of electronic ρ oscillations induced due to the wave properties of an electron. The frequencies $\omega_z^{\rm osc}$, $\omega_\rho^{(1)}$, and $\omega_\rho^{(2)}$ do not change during dissociation of $H_2{}^+$ and HD^+ excited above the dissociation threshold.

The main difference between post-laser-pulse electronic oscillations in homonuclear $H_2{}^+$ and its heteronuclear isotope HD^+ is as follows. Fast post-laser-pulse electronic z oscillations in $H_2{}^+$ are regularly shaped with the period $\tau_{\rm shp} \approx 30$ fs corresponding to nuclear oscillations in $H_2{}^+$. In contrast, since inversion symmetry in heteronuclear HD^+ is broken for both electronic and nuclear motion, electronic z oscillations appear as "echo pulses" of the initial excitation arising with the period of $\tau_{\rm echo} \approx 80$ fs corresponding to nuclear motion in HD^+. Electronic ρ oscillations in HD^+ are also presented by "echo pulses" similar to those of its z oscillations [Fig. 6(e)]. In contrast, electronic ρ oscillations in $H_2{}^+$ first appear just after the end of the laser pulse as regularly shaped with the period of $\tau_{\rm shp} \approx 30$ fs [Fig. 6(b)]. They are followed by an "echo pulse" arising at $t \approx 120$ fs and by regularly shaped ρ oscillations again.

While in the recollision model of Corkum [1], the frequency of electron recollisions with a parent ion is defined by the carrier frequency ω_l of a long laser pulse containing many optical cycles, in the present case of short one-cycle laser pulses, the frequencies of multiple post-laser-pulse recollisions of an electron and nuclei are defined by characteristic frequencies $\omega_z^{\rm osc}$, $\omega_\rho^{(1)}$, and $\omega_\rho^{(2)}$, which manifest themselves by strong spectral lines in the electronic power spectra of $H_2{}^+$ and HD^+.

In contrast, in power spectra of nuclear motion, spectral lines corresponding to $\omega_z^{\rm osc}$, $\omega_\rho^{(1)}$, and $\omega_\rho^{(2)}$ are very weak as compared to low-frequency lines related to nuclear oscillations themselves: $\omega_{\rm shp}$, related to temporal shaping of electronic z oscillations due to nuclear motion in homonuclear $H_2{}^+$, and $\omega_{\rm echo}$, related to the appearance of "echo pulses" during electronic z and ρ oscillations due to nuclear motion in heteronuclear HD^+.

It is shown that the rationalized definition of the harmonic order as $\omega/\omega_z^{\rm osc}$, instead of commonly used for long laser pulses definition ω/ω_l, brings power spectra of electronic z oscillations, mainly generated, as in the present case, during the post-laser-pulse free evolution, in a good agreement with the concept of inversion symmetry of electronic motion in diatomic molecules [5]. Moreover, both definitions are equivalent in the sense that harmonic frequency ω is measured in terms of the frequency of electronic z oscillations in both cases.

Note, finally, that the appearance of post-laser-pulse electronic oscillations is a quite general phenomenon: it always occurs when a laser pulse used does not prepare an eigenstate of the excited system due to nonadiabatic effects caused, e.g., by too fast rise and fall of the laser electric field at the beginning and at the end of a very short laser pulse.

[1] P. B. Corkum, Phys. Rev. Lett. **71**, 1994 (1993).
[2] M. Lewenstein, Ph. Balcou, M. Yu. Ivanov, A. L'Huillier, and P. B. Corkum, Phys. Rev. A **49**, 2117 (1994).
[3] G. K. Paramonov, Chem. Phys. Lett. **411**, 350 (2005).
[4] G. K. Paramonov, Chem. Phys. **338**, 329 (2007).
[5] T. Kreibich, M. Lein, V. Engel, and E. K. U. Gross, Phys. Rev. Lett. **87**, 103901 (2001).
[6] X.-B. Bian and A. D. Bandrauk, Phys. Rev. Lett. **113**, 193901 (2014).
[7] S. Odžak, E. Hasović, and D. B. Milošević, Phys. Rev. A **93**, 043413 (2016).
[8] P. B. Corkum, Phys. Today **64**(3), 36 (2011).
[9] T. Bredtmann, S. Chelkowski, and A. D. Bandrauk, J. Phys. Chem. A **116**, 11398 (2012).
[10] A. D. Bandrauk and G. K. Paramonov, Int. J. Mod. Phys. E **23**, 1430014 (2014).
[11] G. K. Paramonov, O. Kühn, and A. D. Bandrauk, J. Phys. Chem. A **120**, 3175 (2016).
[12] G. K. Paramonov, O. Kühn, and A. D. Bandrauk, Mol. Phys. **115**, 1846 (2017).
[13] A. Shahbaz, C. Müller, A. Staudt, T. J. Bürvenich, and C. H. Keitel, Phys. Rev. Lett. **98**, 263901 (2007).
[14] A. Carrington, I. R. McNab, and C. A. Montgomerie, J. Phys. B: At., Mol. Opt. Phys. **22**, 3551 (1989).
[15] P. J. Mohr, D. B. Newell, and B. N. Taylor, Rev. Mod. Phys. **88**, 035009 (2016).
[16] E. Goulielmakis, M. Schultze, M. Hofstetter, V. S. Yakovlev, J. Gagnon, M. Uiberacker, A. L. Aquila, E. M. Gullikson, D. T. Attwood, R. Kienberger, F. Krausz, and U. Kleineberg, Science **320**, 1614 (2008).
[17] F. Reiter, U. Graf, E. E. Serebryannikov, W. Schweinberger, M. Fiess, M. Schultze, A. M. Azzeer, R. Kienberger, F. Krausz, A. M. Zheltikov, and E. Goulielmakis, Phys. Rev. Lett. **105**, 243902 (2010).
[18] M. Kaluža, J. T. Muckerman, P. Gross, and H. Rabitz, J. Chem. Phys. **100**, 4211 (1994).
[19] V. N. Bagratashvili, Y. G. Vainer, V. S. Doljikov, V. S. Letokhov, A. A. Makarov, L. P. Malyavkin, E. A. Ryabov, and E. G. Silkis, Opt. Lett. **6**, 148 (1981).
[20] P. Salières, P. Antoine, A. de Bohan, and M. Lewenstein, Phys. Rev. Lett. **81**, 5544 (1998).
[21] S. Jiang, C. Yu, G. Yuan, T. Wu, and R. Lu, Sci. Rep. **7**, 42086 (2017).
[22] N. T. Nguyen, T. T. Le, and N. L. Phan, Comput. Theor. Chem. **1094**, 8 (2016).
[23] N. T. Nguyen, V. H. Hoang, and V. H. Le, Phys. Rev. A **88**, 023824 (2013).
[24] N. Takemoto and A. Becker, Phys. Rev. Lett. **105**, 203004 (2010).
[25] M. Haertelt, X.-B. Bian, M. Spanner, A. Staudte, and P. B. Corkum, Phys. Rev. Lett. **116**, 133001 (2016).
[26] X.-B. Bian and A. D. Bandrauk, Phys. Rev. Lett. **108**, 263003 (2012).
[27] Y. Hijikata, H. Nakashima, and H. Nakatsuji, J. Chem. Phys. **130**, 024102 (2009).
[28] G. K. Paramonov and O. Kühn, J. Phys. Chem. A **116**, 11388 (2012).